Energy Conversion and Management 365 (2026) 121724

Contents lists available at ScienceDirect

Energy Conversion and Management

journal homepage: www.elsevier.com/locate/enconman

A simulation-based approach to assess the energy consumption and operational feasibility of hydrogen-powered port equipment

Tobias Prieß *, Luka Bornemann, Martin Kaltschmitt

Institute of Environmental Technology and Energy Economics (IUE), Hamburg University of Technology (TUHH), Eissendorfer Straße 40, 21073 Hamburg, Germany

ARTICLE INFO

Keywords:
Straddle carrier
Terminal tractor
Port decarbonisation
Cargo handling equipment
Zero-emission vehicles
Fuel cell electric vehicles
Feasibility

ABSTRACT

Replacing diesel-powered container handling equipment with zero-emission drivetrains offers major environmental benefits but raises concerns about operational feasibility. This work introduces a scalable simulation approach based on graph networks to estimate the energy consumption of container handling equipment. The method is employed to assess how operational conditions and vehicle configurations influence the operational feasibility for hydrogen-powered terminal tractors and straddle carriers. A systematic parameter variation examines the influence of driver behaviour, operational factors, and technical specifications on energy demand and operational range. Results indicate that hydrogen fuel cell systems can meet individual performance requirements of container terminal operations. Payload and driver behaviour govern the energy consumption, while tailoring tank and battery sizes to the intended application enhances feasibility. The findings provide guidance for designing and operating zero-emission container handling equipment in diverse terminal environments.

1. Background and goal

Diesel-powered container handling equipment (CHE) in German seaports emitted over 150 kt of carbon dioxide (CO_2) in 2021, and the respective CO_2 emissions are expected to increase to ca. 200 kt by 2040 [1]. Globally, more than 100,000 CHE units are in operation, responsible for the emission of 10 to 15 Mt/a of CO_2 [2]. In addition, these devices also emit nitrogen oxides, sulphur oxides, and particulate matter, and are also a source of noise emissions [1].

To reduce the environmental impact of CHE units, fully electrified drivetrains (i.e., fuel cell electric vehicles or battery electric vehicles) can be employed. Such technical solutions offer several advantages compared to the currently used diesel-powered units, as they do not produce local emissions, can achieve higher efficiencies and enable the recuperation of kinetic energy [3].

However, despite these benefits, such electrified powertrains see limited use within terminal environments so far. In Germany, approximately 7 % of the mobile CHE units in duty were powered by alternative powertrains as of 2021, and the majority of this share is attributable to the high electrification rate of automated guided vehicles, over 80 % of which are battery-electric [1].

To enable a broader adoption of zero-emission CHE units in the future, several key prerequisites must be fulfilled.

- Zero-emission powertrain options must be available on the market and technologically mature [1].
- CHE units need to be able to reliably meet given operational demands at the respective terminal. The operational processes must not be disrupted by constraints associated with fleet electrification [4]; i.e., vehicles must not be taken out of operation for recharging or refuelling. In this context, the achievable operational range becomes a decisive factor.
- Finally, the respective technology option needs to be economically feasible [3].

In recent years, equipment manufacturers have developed electric vehicles across all categories of CHE. Based on current TRL assessments [1,5], the availability of zero-emission powertrain options is therefore

Abbreviations: CHE, Container Handling Equipment; CO_2, Carbon Dioxide; ECH, Empty Container Handler; EMS, Energy Management Strategy; OOG, Out-of-Gauge; RS, Reach Stacker; SC, Straddle Carrier; SOC, State of Charge; SOF, State of Fuel; STS, Ship-to-Shore Crane; TT, Terminal Tractor; VRP, Vehicle Routing Problem.

* Corresponding author.
E-mail address: tobias.priess@tuhh.de (T. Prieß).

https://doi.org/10.1016/j.enconman.2026.121724
Received 16 September 2025; Received in revised form 28 April 2026; Accepted 26 May 2026
Available online 13 June 2026

not expected to be a major barrier for the adoption of clean powertrain technologies.

However, the key prerequisite "operational feasibility of zero-emission powertrains" is difficult to evaluate. Research on the feasibility of such powertrains within the heavy-duty sector has primarily focused on trucks so far [6]. In this area, extensive research on the influence of different use cases as well as technological and operational factors on the feasibility of zero-emission powertrains is available. For instance, Forrest et al. [7] evaluated the technical feasibility for the medium and heavy-duty sector in California, while Link and Plötz [8] analysed real-world case studies for regional delivery in Germany. Additionally, Tanvir et al. [9] focused on operational constraints for drayage applications. Furthermore, detailed assessments on the energy consumption of heavy-duty trucks have been carried out (e.g., [10]). Research in this area can rely on test data and standardised test cycles (e.g., the VECTO cycles for regional delivery and long-haul applications) [10].

In contrast, comparable research for CHE units remains scarce. Due to highly diverse equipment types, different operational patterns, and varying terminal layouts [3,6], standardised load cycles for CHE units are not available to date [11], and most likely also in the years to come, resulting in a complicated systematic evaluation.

The influence of different use cases and operating conditions becomes evident in the few cases where energy or fuel consumption values are available from literature [5,12–20] or equipment manufacturers such as Kalmar [21–23], Sany [24,25] and Liebherr [26]. The available values span a wide range (Fig. 1). As the average hourly energy consumption directly determines how long a device can operate without refuelling or recharging, it also governs the achievable operational range, which has previously been identified as a critical measure for evaluating the feasibility of alternative powertrain technologies for CHE units.

Based on the reported values, the impact of varying operational conditions on energy demand and consequently on the feasibility of zero-emission powertrains across diverse use cases remains insufficiently understood. Therefore, there is a need to evaluate which factors influence the energy consumption of CHE units.

Research on the energy demand and feasibility of container handling equipment largely relies on measured data and is typically focused on single use cases for one device type. For instance, Driesch [3] and Di Ilio et al. [12,13] focused their investigations on terminal tractors, while Kukkaro [11] and Hangga and Shinoda [15] analysed straddle carriers. However, analysing the impact of different utilisation scenarios using this approach would require extensive testing under each specific condition, which is time-consuming and costly [15].

To overcome the current limitations of fragmented, single-use-case assessments, this paper presents a novel approach for estimating the energy consumption of CHE units by integrating technical vehicle specifications, terminal-specific operational factors, and driver behaviour into a single framework. This integrated perspective is required because the terminal type and the driver behaviour influence the power demand profile, and the technical specifications govern the final energy consumption required to meet the demand. By replacing extensive physical testing with a graph-based simulation, this study offers the following main contributions.

- A scalable simulation framework: A method generating diverse driving cycles based on a graph network representation of terminal layouts is introduced. This eliminates the need for large-scale physical testing, enabling broader scenario coverage with reduced resource requirements.
- Generalisable feasibility assessment: Unlike studies focused on single-vehicle test data, this approach provides generalisable insights into the operational feasibility of zero-emission equipment across different terminal types and utilisation scenarios.
- Parameter identification: The key operational conditions determining whether currently available zero-emission configurations can serve as viable alternatives to diesel equipment are identified, using the operational range as the central metric of feasibility. While the analysis is realised for hydrogen-fuelled vehicles, the method is easily adaptable to other drivetrain types (e.g., battery-electric systems).

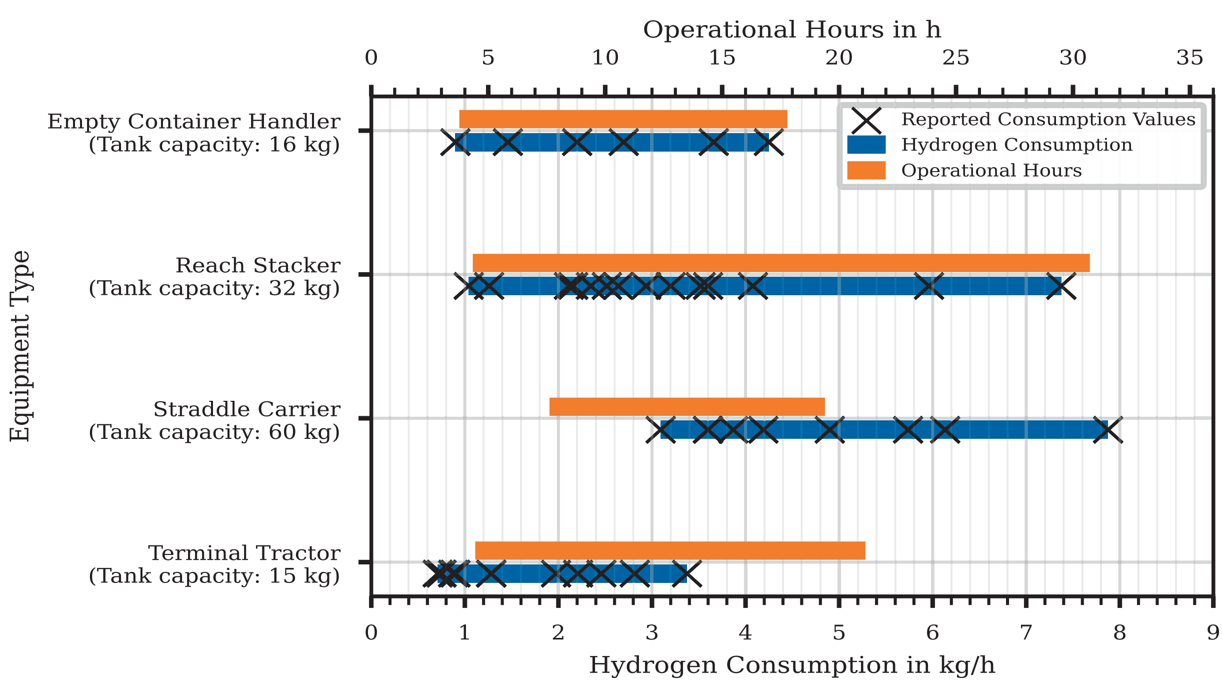

Fig. 1. Hydrogen consumption and resulting operational range for different device types (if energy consumption was given as electrical energy consumption, the value was converted by assuming a fuel cell efficiency of 60 % and the lower heating value of hydrogen, if energy consumption was available as diesel consumption, the value was converted by assuming a 35 % efficiency of the internal combustion engine and the lower heating value of the diesel fuel [13]; reach stacker combines empty and full configurations; terminal tractor includes values for 4x2 and 4x4 configurations; values from [5,12–28].

The remainder of this article is organised as follows: Section 2 details the methodological framework, including the vehicle modelling and energy management strategy. Section 3 describes the reference terminal scenarios and vehicle parameters, and Section 4 presents the simulation results. Finally, Section 5 summarises the key findings and outlines directions for future research.

2. Methodology

To assess zero-emission container handling equipment (CHE), a two-step methodology is developed. The assessment builds on a set of input parameters, including terminal characteristics (e.g., layout), driver behaviour (e.g., acceleration patterns and velocity limits), and vehicle specifications (e.g., motor power, hydrogen tank size). An overview of the method is provided in Fig. 2.

- The first methodological step involves the generation of driving cycles. Such a driving cycle is typically defined as a vehicle speed profile over a certain timeframe [29]. To generate these profiles, the respective terminal layout is transformed into a graph network representation (Section 2.1). This representation, in combination with a defined use case representing the tasks a vehicle faces throughout a shift, and the driver behaviour, characterised mainly by acceleration, deceleration and maximum velocity, enables the creation of driving cycles. In addition to speed profiles, corresponding acceleration, slope, and total vehicle weight profiles are generated within this methodological step.
- In the second step, the corresponding energy consumption is estimated based on the driving cycles using a vehicle model (Section 2.2). The energy consumption and the respective vehicle-specific parameters are used to compute the state of charge of the battery and the state of fuel of the hydrogen tank over time.

Based on this two-step methodology, the operational range of a CHE unit is determined through iterative simulation. After each generated driving cycle, the corresponding energy consumption is evaluated, and the vehicle's energy state (i.e., hydrogen tank level, battery state of charge) is updated. As long as sufficient reserves remain, the next driving cycle is generated and assessed. This process continues until the energy reserves of the respective CHE unit are depleted, at which point the total operating time defines the vehicle's achievable operational range. The operational range is established as the key measure for assessing operational feasibility and therefore serves as the main output of the analysis, since zero-emission equipment must be able to complete full shifts without interruptions for refuelling or recharging to serve as a practical alternative to diesel-powered units [4].

2.1. Graph network simulation for driving cycle generation

Approaches for solving vehicle routing problems (VRP) aim to determine the minimum-cost routes for vehicles or vehicle fleets serving a set of customers [30]. Such methods enable the analysis of the influences of driver behaviour, different vehicle specifications, as well as road management features [31]. Conventional VRPs can be extended to electric vehicle routing problems to determine the route with the lowest energy consumption [32] while considering constraints like range limitations and recharging of vehicles [33]. To solve such VRPs, graph networks are widely used. For example, Goeke and Schneider [30] utilised them to route mixed fleets of electric and conventional vehicles, while Pelletier et al. [34] applied them to account for energy consumption uncertainty.

Compared to such a conventional (electric) VRP, the method presented here diverges in its primary objective. Rather than optimising vehicle routes, the method applies only the energy consumption estimation component of the VRP. The graph network is leveraged to systematically represent the CHE unit movement and operational tasks for the estimation of energy consumption under different terminal-specific conditions (e.g., terminal layout and used equipment, shift structure, driver behaviour, vehicle specification).

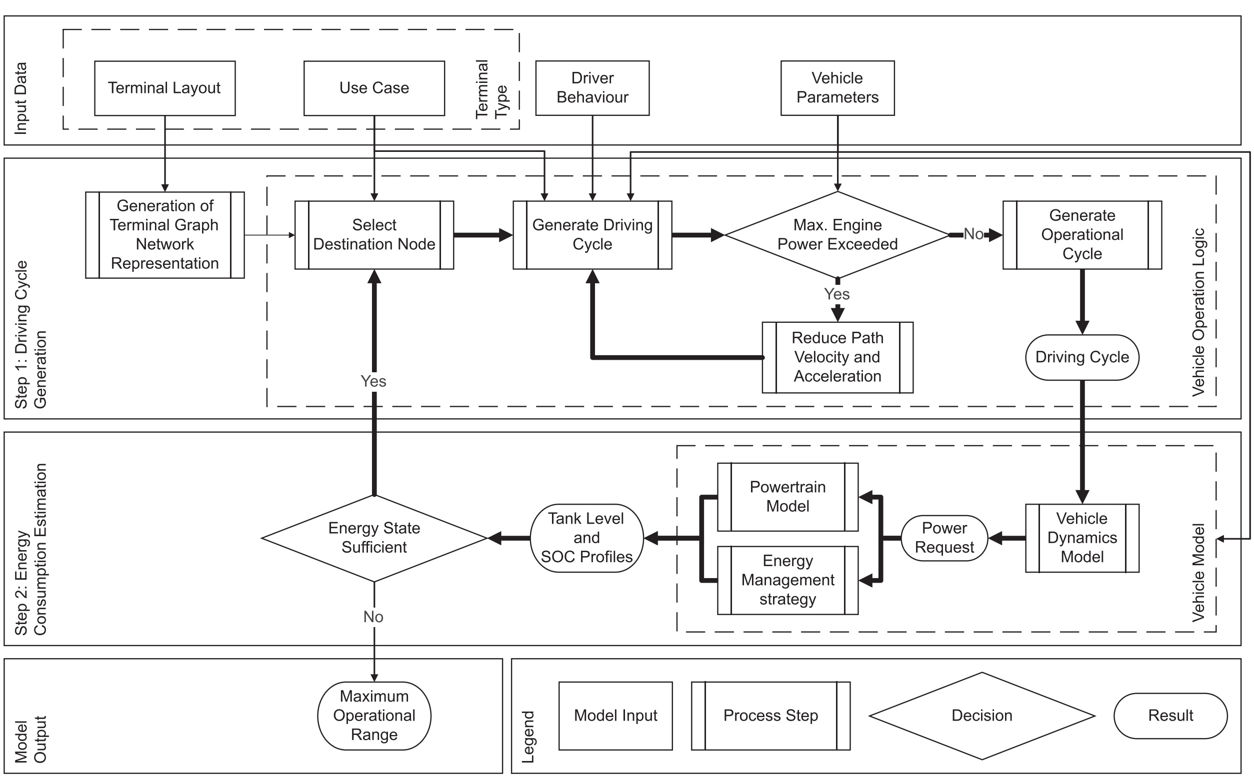

Fig. 2. Methodology for the analysis of the operational range of container handling equipment.

2.1.1. Graph network representation of container terminals

The foundation for the graph network-based energy consumption estimation is the representation of the terminal layout as a graph consisting of edges and nodes. Edges represent roads and nodes represent intersections [32]. Representing the container terminal network requires two node types.

- Routing nodes act as intersections, being necessary to reflect the layout of the terminal and enable the routing of the vehicles between the different operational nodes.
- Operational nodes correspond to locations where container handling activities occur (e.g., container pick-up or drop-off at quay or yard cranes). These operational nodes also include the infrastructure nodes representing the location of refuelling or charging equipment.

Each node has several attributes, including a defined location in a three-dimensional coordinate system and the nodes it is connected to. Based on these attributes, the edges of the graph can be constructed. In addition, the edge characteristics needed for the routing algorithm (e.g., distance and road grade) are determined. The edges denote feasible paths for CHE unit movement between nodes based on the operational connectivity of the terminal. By that, it can be ensured that the CHE unit cannot take blocked routes.

2.1.2. Vehicle operation logic

Once the terminal layout is established through the graph network representation, the next step defines how CHE units operate within this framework. The operational behaviour of the CHE unit is governed by a sequential decision-making process determining equipment actions. This process addresses how individual CHE units navigate through their operational sequences while adhering to energy and operational requirements. The main elements of the operation logic are displayed in Fig. 2.

The vehicle operation is defined by a so-called use case, determining the permissible operational node types a CHE unit can visit and the probability distribution for the different node types. To generate a new driving step, a destination operational node type is selected (see 'Select Destination Node' block in Fig. 2) based on the use case definition, the current node type and the vehicle loading status. Once the target node type is determined, a specific destination node is selected randomly from the available nodes of that type. While the selection within the target type is stochastic, the movement is confined to the valid operational flow defined by the terminal's logistical process. This approach captures the high variability of job assignments across the entire terminal area. Although it does not explicitly model spatial optimisation strategies (e.g., dividing the fleet to service specific sub-zones), this method provides a robust estimation of energy consumption by including longer driving distances that may occur during peak utilisation or unoptimized dispatching. The route between the start and end node is calculated assuming that the vehicle takes the shortest path between the two nodes. The shortest path is determined with the Dijkstra algorithm [35]. Based on the respective route, the complete driving cycle for the step is generated, encompassing both the driving cycle (movement between nodes) and the operational cycle (activities performed at the destination node), as explained in Sections 2.1.3 and 2.1.4. Since both the node type and the specific node selections are randomised, the routes taken by each vehicle during operation might vary, even across identical use cases. This effect intensifies in terminals with a high number of nodes of the same type. The driving distances between different node pairs can differ significantly, leading to differences in the energy consumption. As a result, some randomness is inherent in the model, and outcomes may fluctuate under otherwise identical conditions. Afterwards, the generated step is executed. The vehicle status is then updated, and the procedure iterates with the generation and evaluation of the next step.

Prior to generating a new operational step, the model evaluates the vehicle's current energy state, i.e., hydrogen tank state of fuel (SOF) and battery state of charge (SOC) (decision diamond 'Energy State Sufficient' in Fig. 2). If the energy reserves are insufficient, indicated by the defined minimum state of fuel (SOF_{min}) and minimum state of charge (SOC_{min}) thresholds, no further steps are generated, and the cumulative time is recorded as the vehicle's operational range. Conversely, if the reserves are sufficient, a new step is generated and the simulation continues.

2.1.3. Driving cycle generation

To generate the velocity profile along the identified route, train-like speed profiles are adopted along the edges. This approach is consistent with existing approaches (e.g., [33,36]), where energy consumption is estimated based on speed profiles.

For each edge, the velocity profile consists of an acceleration phase, a cruising phase and a deceleration phase.

- In the acceleration phase, a constant acceleration is considered until the CHE unit reaches the target cruising speed.
- Afterwards, the CHE unit enters a phase where it maintains a constant velocity until the deceleration phase begins.
- In the deceleration phase, the vehicle reduces its velocity with a constant deceleration until it reaches the defined end velocity.

The start and end velocities can vary depending on the node type. At the start node of the path, the CHE unit has a velocity of 0 km/h by definition. When reaching the final node of the route, the vehicle must have a velocity of 0 km/h as well to carry out the operation. If the end node of the edge is a routing node where the vehicle has to make a turn, the end velocity is a random value between 0 and 50 % of the cruising velocity to consider the turning of the vehicle around corners. If the direction stays the same, the vehicle does not need to lower its velocity. When generating the speed profiles along an edge, two different aspects are always checked.

- If the cruising velocity cannot be reached due to an insufficient edge length, the cruising velocity for that edge is reduced and the profile is calculated again until a reasonable driving velocity is determined.
- If the maximum motor power the vehicle can provide is exceeded at any point of an edge (decision diamond 'Max. Engine Power Exceeded' in Fig. 2), the acceleration and deceleration values, as well as the driving velocity, are reduced for the edge until the maximum power can be supplied by the respective motor.

After the generation of the velocity profile for the route, the profile is smoothed over a rolling window size of 2 s. The time step size of the generated profiles is 0.25 s. Afterwards, the acceleration is calculated as the gradient of the velocity profile. It is also assumed that the CHE unit only drives forward [3]. As a simplification, interactions of vehicles (e.g., traffic congestion) are not considered.

Example driving cycles generated using the presented approach are presented in Appendix A.

2.1.4. Generation of operational cycles

Beyond the horizontal driving movement along the route, equipment-specific operational cycles are needed to capture the full range of activities performed by CHE units. These cycles are particularly important for active vehicles (e.g., straddle carriers), which are defined by their capability to perform lifting or stacking operations, in contrast to passive devices (e.g., terminal tractors), which are restricted to horizontal transport [37].

To achieve that, driving profiles consisting of speed profiles and, if applicable, lifting-related profiles like the lifting velocity, are generated after reaching the operational node (see 'Generate Operational Cycle' in

Fig. 2). These activities need to be defined and described as discrete actions for each CHE unit type. The possible operational tasks include driving manoeuvres like queuing or approaching a container, waiting (e.g., for the crane to place a container), and lifting or lowering movements.

For lifting operations, the system models vertical movements using similar dynamic principles applied to the horizontal motion. The lifting movement to the specified height is therefore also divided into an acceleration, cruising and deceleration phase. For simplification, needed adjustments of spreader positions are neglected. This simplification is justified as container adjustments account for less than 10 % of the working time and energy consumption of a straddle carrier [15] and it is assumed that this behaviour can be transferred to all active CHE devices.

Appendix A provides example operational cycles illustrating the resulting speed and lifting profiles.

2.2. Estimation of energy consumption

To calculate the energy consumption based on the generated driving cycles, a backwards-facing vehicle model is utilised. Based on velocity, acceleration, vehicle weight and road slope profiles, the resulting power request can be estimated ('Step 2: Energy Consumption Estimation' in Fig. 2) [38]. Integrating the instantaneous power demand over the driving cycle yields the total energy consumption.

2.2.1. Vehicle dynamics model

The total resistance force F_r that the vehicle faces while driving results from the aerodynamic resistance, the rolling friction and the grading resistance. The traction power P_w required at the wheels to overcome this resistance force can be calculated based on Equation (1) [12,13,38].

$$P_w = F_r v P_w = 0.5\rho v^3 A_v c_d + m_v g v[f_{roll} cos\alpha + sin\alpha] + \delta m_v a v \tag{1}$$

The air density ρ, the gravitational acceleration g, the drag coefficient c_d and the mass factor δ are constants (see Table 2 for definition). The vehicle velocity v, the vehicle frontal area A_v, the total mass of the vehicle m_v, the vehicle acceleration a, the road slope α and the rolling resistance coefficient f_{roll} might change over time. The profiles for all time-dependent variables are generated during the driving cycle synthesis (Sections 2.1.3 and 2.1.4), examples of which are illustrated in Appendix A to demonstrate the resulting kinematics and load profiles. Consequently, the variables in Equation (1) are directly determined by the operational inputs: the total vehicle mass incorporates the payload, while the velocity and acceleration profiles are governed by the driver behaviour constraints (i.e., maximum allowed speed and acceleration rates defined in Table 3 and Table 4). This ensures that variations in driver aggressiveness or cargo weight are translated into specific power requests through the physical resistance forces of the model.

In the case of active devices, the power needed for lifting movements, P_{lift}, needs to be considered as well (Equation (2)). The lifted mass m_{lift}, considering the spreader and the load, and the lifting velocity v_{lift} are determined during the driving cycle synthesis [39].

$$P_{lift} = m_{lift} g v_{lift} \tag{2}$$

To calculate the required electric motor power for driving, $P_{m,drive}$ (Equation (3)), an average drivetrain (η_t) and motor efficiency (η_{EM}) are assumed [12,13,38].

$$P_{m,drive} = P_w(\eta_t \eta_{EM})^{-sgn(P_w)} \tag{3}$$

To calculate the power request for lifting movements, $P_{m,lift}$ (Equation (4)), a lifting efficiency (η_{lift}) is taken into account [39].

$$P_{m,lift} = P_{lift}(\eta_{lift}\eta_{EM})^{-sgn(P_{lift})} \tag{4}$$

The total power requested from the power source, P_{el} (Equation (5)), also takes the power consumption of the auxiliary loads P_{aux} into account [38].

$$P_{el} = P_{aux} + P_{m,drive} + P_{m,lift} \tag{5}$$

2.2.2. Energy management strategy

The total requested power (P_{el}) by the CHE unit is supplied by the fuel cell (P_{FC}) and the battery (P_{bat}) (Equation (6)). A DC/DC converter (converter efficiency η_{DCDC}) connects the fuel cell (FC) to the high voltage bus. Motor and battery are directly connected to the high-voltage bus, as illustrated in Fig. 3 [13].

$$P_{el} = P_{FC}\eta_{DCDC} + P_{bat} \tag{6}$$

To govern the power distribution between the fuel cell and the battery, a rule-based energy management strategy (EMS) based on [40] is implemented. While recent research often explores data-driven energy management strategies, a rule-based EMS was deliberately selected for this study to ensure broad applicability across diverse equipment types and configurations.

The system aims to keep the battery state of charge (SOC) in a defined range between an upper (SOC_{high}) and lower (SOC_{low}) limit and switches the fuel cell off when a defined maximum SOC (SOC_{max}) limit is exceeded. If the SOC is below SOC_{max}, the fuel cell power output is determined based on the requested load power (P_{el}), the SOC, and the fuel cell minimum ($P_{FC,\min}$), optimum ($P_{FC,opt}$) and maximum ($P_{FC,\max}$) power outputs. In addition, the battery characteristics, i.e., the battery capacity (E_{bat}) and the optimum discharge ($C_{opt,dis}$), charge ($C_{opt,cha}$) and optimum (C_{opt}) C-rates, are considered as the goal of the EMS is to optimise the system's efficiency [40]. The resulting logic, summarised in Table 1, defines 12 operational states.

- Fuel Cell Deactivation (State 0): When the battery is overcharged (SOC $>$ SOC_{max}), the fuel cell is turned off to prioritise battery depletion.
- Minimum Power Operation (States 1, 2, 5): The fuel cell operates at its minimum power ($P_{FC,\min}$) when the SOC is normal or high (SOC_{low} $<$ SOC $<$ SOC_{max}) and the required load power is low.
- Maximum Power Operation (States 4, 9, 11): During periods of high power demand or when the battery SOC drops below the critical threshold (SOC $<$ SOC_{low}), the fuel cell operates at its maximum rated power ($P_{FC,\max}$). This ensures the load is met while simultaneously recharging the battery to prevent depletion.
- Load Following (States 3, 6, 8, 10): In intermediate conditions where the system cannot efficiently operate at a fixed point, the fuel cell output is regulated to follow the load power ($P_{FC} \approx P_{el}$), utilising the battery to buffer minor fluctuations.
- Optimum Power Operation (State 7): State 7 represents the ideal operating condition. The fuel cell is locked to its optimum operating point ($P_{FC,opt}$). This state is activated when the load demand (P_{el}) falls within a specific window around $P_{FC,opt}$, defined by the battery's optimum power capability ($\pm E_{bat}C_{opt}$). Within this bandwidth, the battery efficiently buffers the difference between the varying load and the steady optimal fuel cell output, maximising the system's total efficiency.

2.2.3. Powertrain model

The energy and hydrogen consumption based on the battery and fuel cell power are calculated based on the power requests and a model of the power sources. Here, a simplified representation of the fuel cell and

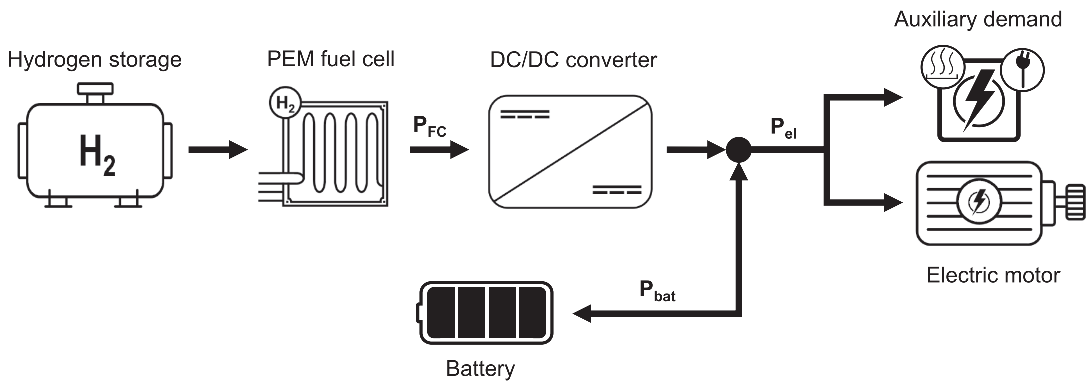

Fig. 3. Configuration of the fuel cell electric energy system (PEM: Polymer electrolyte membrane, P_{el}: Total power request, P_{FC}: Fuel cell power output, P_{bat}: Battery power flow).

Table 1
Summary of the rule-based EMS based on [40].

Battery SOC	State	Load power	Fuel cell power
$SOC > SOC_{max}$	0		0
$SOC_{high} < SOC \leq SOCmax$	1	$P_{el} \leq P_{FC,min}$	$P_{FC,min}$
	2	$P_{FC,min} < P_{el} \leq P_{FC,min} + E_{bat}C_{opt,dis}$	$P_{FC,min}$
	3	$P_{FC,min} + E_{bat}C_{opt,dis} < P_{el} \leq P_{FC,max} + E_{bat}C_{opt,dis}$	$P_{el} - E_{bat}C_{opt,dis}$
	4	$P_{FC,max} + E_{bat}C_{opt,dis} < P_{el}$	$P_{FC,max}$
$SOC_{low} \leq SOC \leq SOC_{high}$	5	$P_{el} \leq P_{FC,min}$	$P_{FC,min}$
	6	$P_{FC,min} < P_{el} \leq P_{Fc,opt} - E_{bat}C_{opt}$	P_{el}
	7	$P_{Fc,opt} - E_{bat}C_{opt} < P_{el} \leq P_{Fc,opt} + E_{bat}C_{opt}$	$P_{Fc,opt}$
	8	$P_{Fc,opt} + E_{bat}C_{opt} < P_{el} \leq P_{FC,max}$	P_{el}
	9	$P_{el} > P_{FC,max}$	$P_{FC,max}$
$SOC < SOC_{low}$	10	$P_{el} \leq P_{FC,max} - E_{bat}C_{opt,cha}$	$P_{el} + E_{bat}C_{opt,cha}$
	11	$P_{el} > P_{FC,max} - E_{bat}C_{opt,cha}$	$P_{FC,max}$

battery system is considered. Due to this simplified efficiency estimation, different fuel cell and battery sizes as well as efficiencies can easily be considered in the model. Power requests from the power source are denoted with a positive sign.

The state of charge change (ΔSOC) based on the power requested or supplied to the battery (P_{bat}) and the efficiency of the battery, η_{bat}, during a time step (Δt) can be calculated according to Equation (7) [12].

$$\Delta SOC = \frac{-P_{bat}\Delta t(\eta_{bat})^{-sgn(P_{bat})}}{E_{bat}} \tag{7}$$

If the peak charge rate of the battery is exceeded in the case of regeneration, it is assumed that the battery is charged at its maximum allowable power, and any excess braking power is dissipated via the mechanical brakes.

The hydrogen mass that is consumed during a timestep, m_{H2}, is calculated based on the power requested from the fuel cell (P_{FC}), the lower heating value LHV_{H2} of the hydrogen fuel and the fuel cell efficiency η_{FC} (Equation (8)) [38].

$$m_{H2} = \frac{P_{FC}\Delta t}{\eta_{FC}LHV_{H2}} \tag{8}$$

The fuel cell efficiency is estimated by a linear approximation as a function of the fuel cell power output P_{FC}. This approximation is defined within the interval $P_{FC} \in [P_{FC,min}, P_{FC,max}]$, where $P_{FC,min}$ corresponds to the minimum operating point under the applied energy management strategy, while $P_{FC,max}$ equals the rated power of the fuel cell and denotes full load. The maximum ($\eta_{FC,max}$) and minimum ($\eta_{FC,min}$) efficiency of the fuel cell correspond to the respective efficiencies at the end points of the interval. Within this interval, the efficiency decreases linearly (Equation (9)).

$$\eta_{FC}(P_{FC}) = \eta_{FC,max} + \left(\frac{\eta_{FC,max} - \eta_{FC,min}}{P_{FC,min} - P_{FC,max}}\right)(P_{FC} - P_{FC,min}) \tag{9}$$

Appendix A illustrates the application of the vehicle dynamics model and energy management strategy through example cycles, showing the resulting power demand profiles and power distribution between the fuel cell and battery for different device types.

3. Case study

Below, the case study to be assessed here is defined. The considered terminal types are elaborated in Section 3.1. The container handling equipment (CHE) types investigated here are described and defined in Section 3.2. The parameter variation carried out to identify the parameters that influence zero-emission CHE unit feasibility is explained in Section 3.3. Each considered configuration was simulated in 10 independent iterations to account for the stochastic variability inherent in the random node selection process. This sample size allows for a robust estimation of the average operational range while providing a clear representation of the result distribution. As illustrated in the results (Section 4), the variance of these iterations is represented through interquartile ranges and whiskers in the box plots, which serve as a visual analysis of the statistical spread and result consistency. The proposed methodological framework (Section 2) was implemented in Python. The graph network operations and shortest path algorithms were executed using the NetworkX library [41].

3.1. Terminal types

To account for the diversity of container terminal configurations and examine how these variations affect the feasibility of zero-emission powertrains, generic reference terminals are employed. These terminals capture the essential features of different terminal archetypes. While individual terminals exhibit unique characteristics, fundamental similarities allow for a systematic categorisation. Each reference terminal is thus defined by three key components.

- The first one is the terminal layout representing the physical arrangement of operational areas (e.g., quayside, storage yards). This layout directly influences the vehicle movement patterns and covered distances. The given terminal layout is then transferred to a graph network representation.
- Additionally, the equipment fleet composition, defining types and quantities of CHE units employed, is defined. This fleet composition may vary significantly across different terminal archetypes and is impacted by several factors (e.g., size of the terminal, cargo type, automation grade). It influences the tasks the different CHE units have to fulfil. For example, if straddle carriers are present, terminal tractors are not needed for the horizontal transport of containers between the quay crane and the yard.
- The last aspect is the operational pattern of the terminal, including the number of shifts per day and the break structure. These patterns influence the number of recharging or refuelling opportunities and the minimum operational range a CHE unit has to be able to fulfil.

The reference terminal approach enables a systematic evaluation of powertrain alternatives across different operational contexts while avoiding the complexity of modelling every possible terminal configuration. By focusing on representative archetypes, the methodology can assess how terminal-specific factors influence the viability of zero-emission technologies and identify the operational conditions under which different powertrain options are most suitable.

Here, two different reference terminals are considered: The flat field terminal and the empty container terminal.

Flat field reference terminal. The graph network representing the flat field terminal layout is displayed in Fig. 4. Containers are discharged from the vessel at the quay (orange nodes in Fig. 4). A 20 % share of empty inbound quay containers is assumed. Four straddle carriers (SC) are assigned to one quay crane. The majority of the flat field terminal area is attributed to the SC yard (green nodes in Fig. 4). Here, containers are stored before they are transferred to the quay cranes, to trucks or to the rail section. These transfer movements are carried out by SCs, as these are the only devices that can enter the yard due to their capability to drive over containers. Therefore, the nodes inside the yard are not connected to the other nodes and can only be approached by SCs.

The terminal is assumed to have an empty container section (red nodes in Fig. 4) that is operated independently. Empty containers are moved between the empty container section and the rest of the terminal by the rail-mounted gantry crane, which is also used to load and unload trains. The empty container transfer at the terminal is carried out with SCs.

The out-of-gauge (OOG) section (pink nodes in Fig. 4) is used to store all types of non-containerised cargo. OOG cargo is transferred to the train (brown nodes in Fig. 4), truck (violet nodes in Fig. 4) and quay (orange nodes in Fig. 4) sections by 4x2 terminal tractors. In addition, full container reach stackers are used at the terminal for the transfer of OOG load between the OOG, truck and rail sections. The idle section (grey nodes in Fig. 4) contains the refuelling infrastructure and parking spots for the vehicles that are not in use.

The terminal operates in three shifts, each with 7:30 h of operation and 30 min breaks between the shifts. Therefore, vehicles need to be able to at least cover an operational range of 8 h.

Empty container reference terminal. The graph network representing the empty container terminal layout is displayed in Fig. 5. The layout considers two yard areas (green nodes in Fig. 5). To accurately reflect the simulated logistics processes, one yard area is modelled in detail to include container stacking and retrieval operations performed by empty container handlers (ECH) and reach stackers (RS), while the second yard area primarily serves to integrate the horizontal transfer movements conducted by terminal tractors (TT). Each yard area can be entered from a road by trucks and TTs. Containers are loaded onto and unloaded from the trailers with empty container RSs and ECHs at dedicated loading positions (violet nodes in Fig. 5). RSs and ECHs are also used to stack and retrieve containers from the yard area. The idle section (grey nodes in Fig. 5) contains infrastructure for charging and

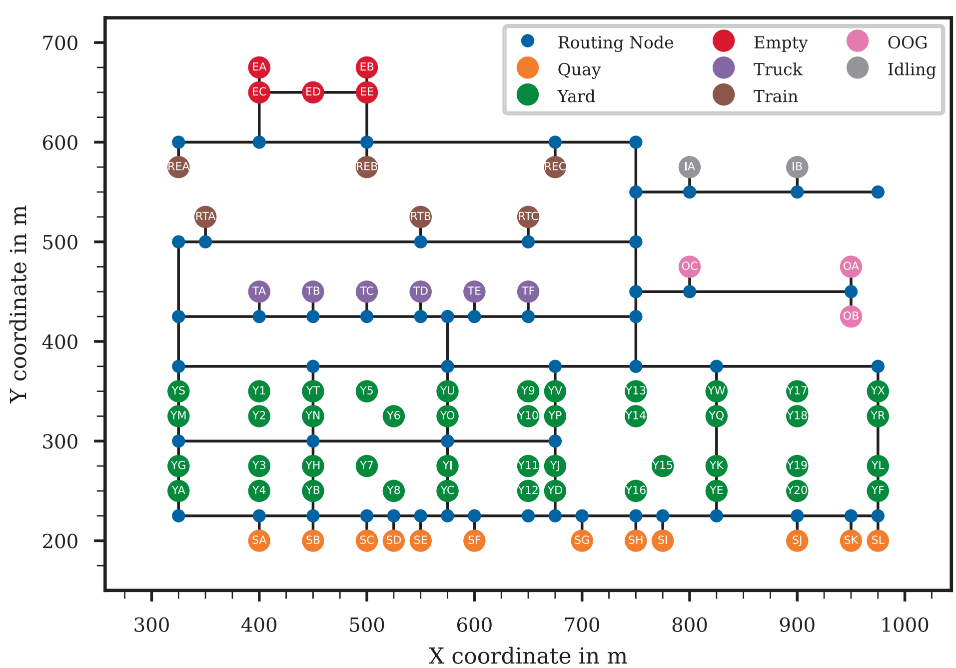

Fig. 4. Graph network representing the flat field terminal layout (OOG: Out-of-gauge).

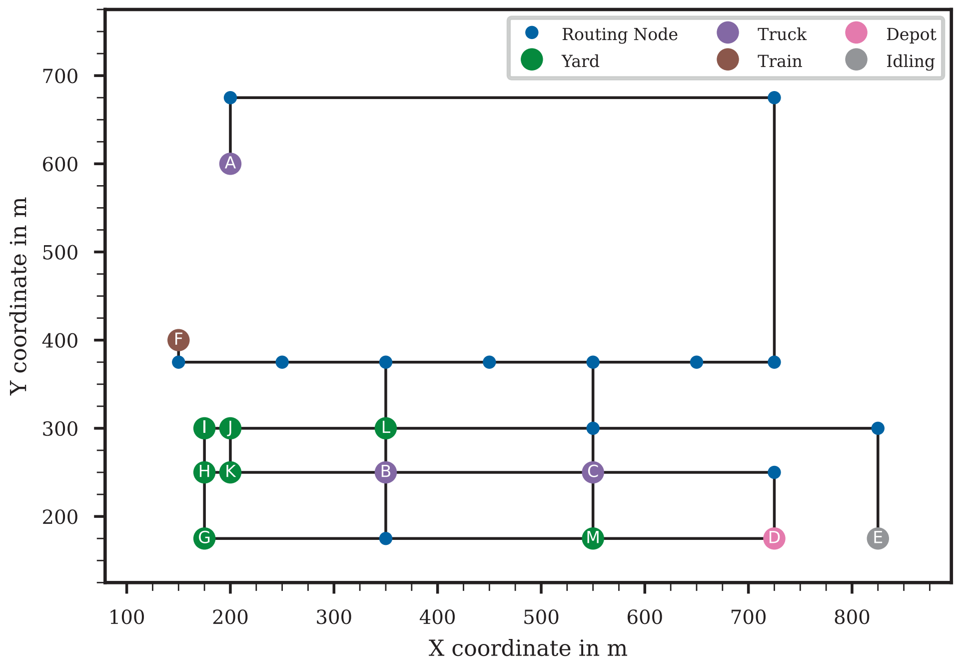

Fig. 5. Graph network representing the empty container terminal layout.

Table 2
General model parameters.

Parameter		Unit	Value	Reference
Empty container weight		t	3.85	[42]
Full container weight		t	22.275	[42]
Out-of-gauge weight		t	20	
Battery efficiency	η_{bat}	%	97	[13]
Battery peak charge rate		C	1.5	[12]
Battery optimum charge rate	$C_{opt,cha}$	C	0.3	[40]
Battery optimum discharge rate	$C_{opt,dis}$	C	0.3	[40]
Battery optimum rate	C_{opt}	C	0.2	[40]
Electric motor efficiency	η_{EM}	%	93	[12]
Drivetrain efficiency	η_{t}	%	92	[13]
DC/DC converter efficiency	η_{DCDC}	%	93	[12]
Drag coefficient	c_d	–	0.8	[12]
Mass factor	δ	–	1.1	[12]
Auxiliary power consumption	P_{aux}	kW	5	[12]
SOC goal range upper limit	SOC_{high}	%	85	
SOC goal range lower limit	SOC_{low}	%	65	
Maximum SOC	SOC_{max}	%	90	
Minimum SOC	SOC_{min}	%	10	
Minimum SOF	SOF_{min}	%	5	
Maximum fuel cell efficiency	$\eta_{FC,\max}$	%	58	[43]
Minimum fuel cell efficiency	$\eta_{FC,\min}$	%	48	[43]
Optimum fuel cell power	$P_{FC,opt}$	% of $P_{FC,\max}$	55	
Minimum fuel cell power	$P_{FC,\min}$	% of $P_{FC,\max}$	17	

Table 3
Terminal tractor model parameters.

Parameter		Unit	Value	Reference
Vehicle weight		t	8.24	[3]
Gooseneck weight		t	3.4	
Bomb-cart trailer weight		t	8	
Chassis weight		t	2.95	[42]
Vehicle frontal area	A_v	m^2	8	[12]
Rolling resistance coefficient vehicle	f_{roll}		0.024	[3,12]
Rolling resistance coefficient vehicle and trailer	f_{roll}		0.015	[3,12]
Maximum velocity		km/h	30	
Maximum acceleration unladen		m/s^2	0.3	
Maximum acceleration laden		m/s^2	0.2	
Maximum deceleration		m/s^2	−0.75	
Maximum power drive motor		kW	230	
Fuel cell rated power	$P_{FC,\max}$	kW	45	
Hydrogen tank capacity		kg	15	
Battery nominal capacity	E_{bat}	kWh	130	

refuelling as well as parking spots.

The terminal operation is divided into two 7:30 h shifts and a 30 min break between the shifts. The minimum operational range that vehicles need to cover is therefore set to 8 h.

Main differences between the terminal types. To conclude the terminal description, the key operational distinctions between the two reference archetypes are summarised. The flat field terminal represents a high-intensity environment characterised by frequent cornering, heavy payloads (OOG cargo and full containers), and continuous 24-hour operation (3 shifts). In contrast, the empty container terminal features a simplified layout with long, straight road sections, lighter payloads (empty containers), and reduced operating hours (2 shifts).

3.2. Devices

To allow for a comparison of active and passive devices, the analysis is carried out for a terminal tractor (TT) and a straddle carrier (SC). Additionally, the inclusion of the TT enables the examination of different terminal types, while the SC is exclusively deployed at the flat field terminal. Model parameters being identical for all analysed vehicles are listed in Table 2.

The main output of the simulation is the operational range, which is defined as the total cumulative operating time before a minimum energy state is reached. Consistent with the methodology described in Section 2.1.2, the simulation terminates if the energy state is below SOF_{min} or SOC_{min} after the completion of the previous step. All vehicles are initialised with a tank level of 90 % and the initial battery charge level is set to the midpoint of the desired state of charge range (75 %).

Table 4
Straddle carrier model parameters.

Parameter		Unit	Value	Reference
Vehicle weight		t	72	
Vehicle frontal area	A_v	m^2	35	
Spreader weight		t	7.2	
Rolling resistance coefficient vehicle	f_{roll}	–	0.018	
Maximum velocity		km/h	24	
Maximum acceleration unladen		m/s^2	0.3	
Maximum acceleration laden		m/s^2	0.2	
Maximum deceleration		m/s^2	−0.75	
Maximum lifting velocity		m/s	0.3	
Maximum lifting acceleration		m/s^2	0.2	
Maximum lifting deceleration		m/s^2	−0.4	
Maximum power drive motor		kW	285	
Maximum power lift motor		kW	150	
Fuel cell rated power	$P_{FC,max}$	kW	150	
Hydrogen tank capacity		kg	60	
Battery nominal capacity	E_{bat}	kWh	130	
Lifting efficiency	η_{lift}	%	85	[39]

3.2.1. Terminal tractor

Terminal tractors (TT) can only be used for horizontal transportation [44] and are available as 4x2 and 4x4 configurations. 4x4 versions are used for heavy-duty services (e.g., in Roll-on / Roll-off terminals) [12]. Here, a 4x2 configuration is analysed. The baseline model parameters for the 4x2 TT model are listed in Table 3.

The operational range of the TT is investigated on the flat field and the empty container terminal. On the flat field terminal, the considered use case is the transfer of out-of-gauge load between the out-of-gauge, train and quay sections. The TT always has a gooseneck connected and can drive empty or with a bomb-cart trailer attached to the gooseneck. The use case on the empty container terminal is the transfer of empty containers between the yard areas. The TT unit always has a chassis connected without a gooseneck.

3.2.2. Straddle carrier

Straddle carriers (SC) can be used for the horizontal transportation, stacking and retrieving of containers and for the loading and unloading of trucks and trains [44]. The baseline model parameters for the SC model are listed in Table 4.

The considered use case for the SC involves transporting full containers between the yard and a certain assigned quay crane, as well as moving empty containers between the train section and the quay cranes.

3.3. Parameter variation

Since the reference terminals differ in aspects such as the terminal layout and the load type, comparing their results already enables the identification of parameters that influence the energy consumption and the operational feasibility of zero-emission container handling equipment units. Beyond these structural differences, a systematic parameter variation is conducted. To capture the impact of the driver behaviour, the maximum allowed acceleration and deceleration are varied. In addition, the effect of limiting driving and lifting velocities is analysed. Besides this, the impact of technical specifications is investigated by adjusting the vehicle weight, the fuel cell efficiency, the battery capacity, and the hydrogen tank size. The ranges of all varied parameters are summarised in Table 5.

Table 5
Ranges of varied parameters expressed as lower and upper percentages relative to the base case values.

Parameter	Terminal tractor		Straddle carrier	
Driver Behaviour				
Maximum vehicle speed	−50	30	−50	10
Maximum acceleration and deceleration	−60	100	−60	100
Maximum lifting velocity			−60	40
Technical Specifications				
Vehicle weight	−10	50		
Hydrogen tank capacity	−30	30		
Maximum fuel cell efficiency	−20	20		
Battery capacity	−75	5		

4. Results and discussion

Below, the simulation results on the operational feasibility and energy consumption of hydrogen-fuelled container handling equipment (CHE) are presented. Based on the results, the key parameters influencing the operational feasibility are identified, and measures to enhance the applicability of zero-emission CHE units are derived. The evaluation first considers the influence of driver behaviour and operational factors, which is examined for both passive and active devices (Section 4.1). Subsequently, the role of technical specifications is analysed for the terminal tractor (Section 4.2).

4.1. Driver behaviour and operational factors

Driver behaviour and operational factors (i.e., payload, terminal layout) represent two influential factors for the operational feasibility of zero-emission CHE units. Acceleration, deceleration and driving velocity dictate the vehicle's power demand, while the payload determines the total vehicle mass and thereby influences the energy consumption. To examine these effects, results are first presented for a passive device, represented by a 4x2 terminal tractor, and subsequently for an active device, represented by a straddle carrier. A combined discussion of the main trends and their implications follows in Section 4.1.2.

4.1.1. Results

Passive Devices. The influence of the driver behaviour on the operational range of a terminal tractor (TT) on the flat field and empty container terminals is shown in Fig. 6. The lowest operational range is slightly above the limit of 8 h and occurs under the most aggressive driver behaviour on the flat field terminal, while the highest operational range of ca. 17 h is reached on the empty terminal at the lowest allowed velocity. Consequently, the vehicle can achieve the requested operational range of 8 h of uninterrupted operation under all conditions. In general, the operational range on the empty container terminal is ca. 2 h longer compared to the flat field terminal. Apart from the differences in absolute runtime, the influence of acceleration, deceleration, and velocity limits exhibits consistent patterns that emerge across both terminal types. The operational range decreases at comparable rates as these parameters increase. Notably, while the slopes of the acceleration and deceleration curves are similar, the velocity curve is steeper on the empty terminal.

The equivalent hydrogen consumption in the base case on the empty container terminal is around 0.35 kg/h lower than on the flat terminal (Fig. B1). In general, the hydrogen consumption across all cases is in the range of 0.7 to 1.7 kg/h and therefore at the lower end of the spectrum reported in Fig. 1. This is expected as values for a 4x4 TT are included there, which experience higher power peaks due to the slope occurring when driving inside of ships.

Active devices. The influence of driver behaviour-related metrics on the operational range of the straddle carrier (SC) is presented in Fig. 7. In addition to the longitudinal acceleration and velocity considered for the TT, the analysis is extended to lifting-related parameters for the SC, focusing on the lifting velocity.

Compared to the TT, the SC exhibits greater variance between iterations of the same configuration, due to the randomness in node selection. This effect is amplified by the high number of yard nodes, which introduces additional variability to the driving cycles, even for identical vehicle configurations. While the influence of acceleration, deceleration, and maximum velocity exhibits analogous behaviour to that observed for passive devices, a notable difference arises, as increases in

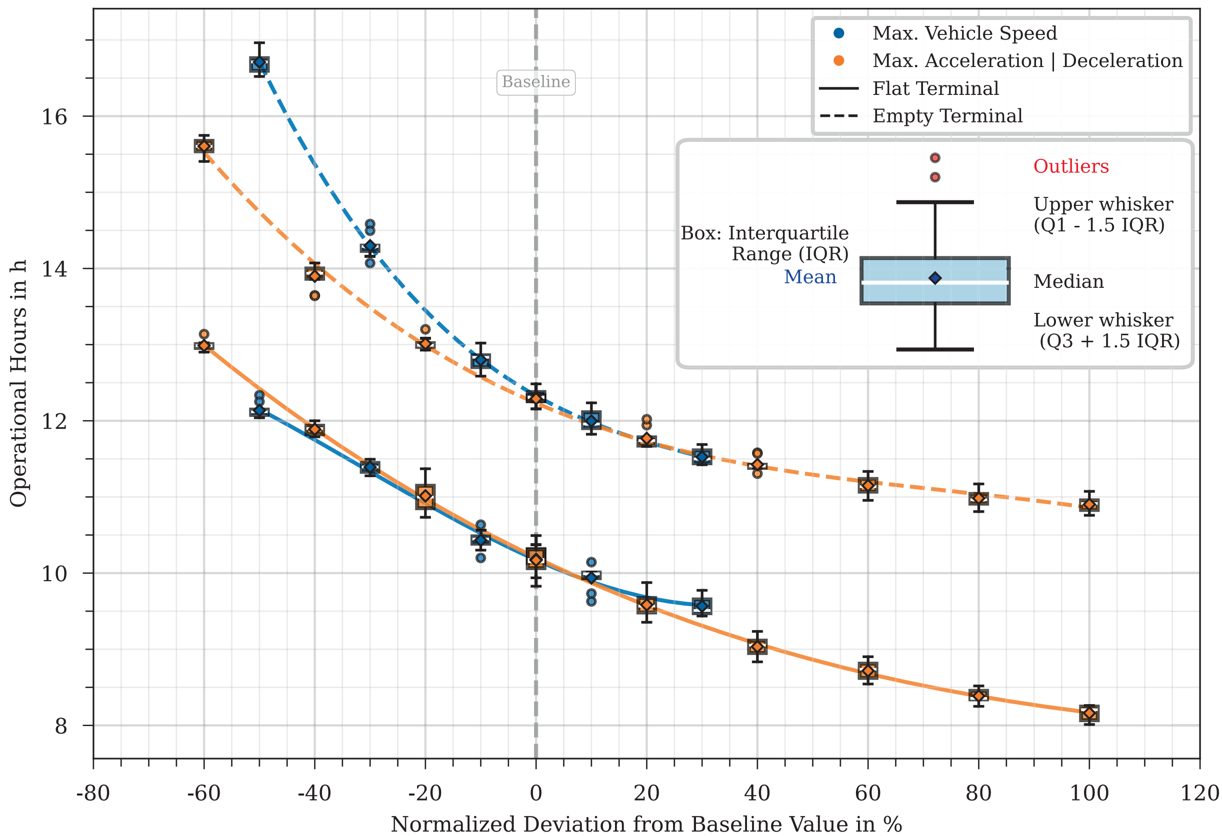

Fig. 6. Influence of the driver behaviour on the operational range of a terminal tractor on a flat field and an empty container terminal. The box plots represent the results of 10 independent iterations.

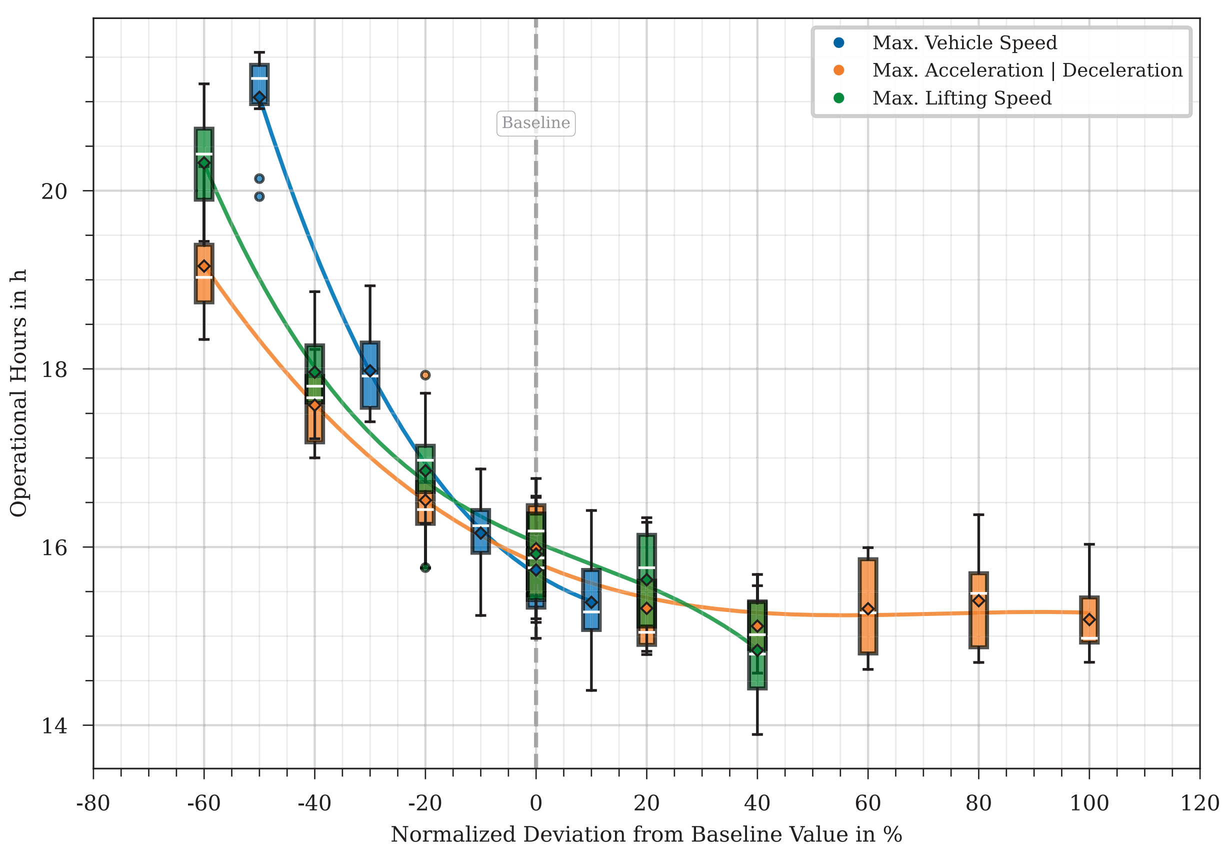

Fig. 7. Influence of driver behaviour on the operational range of a straddle carrier. The box plots represent the results of 10 independent iterations.

acceleration and deceleration limits beyond 20 % do not further reduce the operational range for the SC. Similar to the driving velocity, reducing the lifting velocity also extends the operational range.

The equivalent hydrogen consumption of the SC ranges between 2.4 and 3.6 kg/h (Fig. B2). These values lie at the lower end of the spectrum shown in Fig. 1 and even below the reported values in some cases. This could result from the limited data availability or the favourable conditions assumed in this analysis. Moreover, while validated vehicle models are available for TTs [12,45], no such validated model currently exists for SCs. Nevertheless, the relative influence of the investigated parameters should not be affected, as the same vehicle model was applied for all configurations.

4.1.2. Discussion

Payload. The influence of the payload can be assessed for the terminal tractor (TT) by comparing the results for the empty container terminal with those for the flat field terminal. The higher operational range observed on the empty terminal demonstrates that both the load weight and the total vehicle weight strongly affect the respective energy demand. On the empty terminal, the reduced overall vehicle mass, resulting from a lighter load and the lower weight of the chassis compared to the bomb-cart trailer with a gooseneck, leads to lower energy consumption than in the flat field scenario. The power consumption profiles in Appendix A1 illustrate this difference, with the flat field terminal (Fig. A1) showing higher traction power demands due to the heavier OOG cargo compared to the empty container terminal (Fig. A2). While the payload itself cannot be modified, it remains a critical factor in determining whether a device is suitable for a given use case or terminal configuration.

Driving velocity and acceleration. The effect of the velocity limit on the operational range is evident for both active and passive devices, as an increased velocity limit reduces the operational range for all configurations. While the velocity limit directly impacts the operational range, its effect is further shaped by the specific characteristics of the terminal layout. On the empty container terminal, characterised by long and straight road sections, the vehicle operates at the maximum velocity for extended periods, as illustrated in Fig. A2. When the maximum driving velocity is low, the vehicle correspondingly spends more time driving at this lower speed, resulting in reduced energy consumption. In contrast, the flat field terminal features a higher number of turns, leading to more frequent acceleration and deceleration events. As a result, the influence of the maximum velocity on the operational range is diminished, as reflected by the flatter slope of the velocity curve on the flat field terminal in Fig. 6.

A more aggressive acceleration and deceleration behaviour leads to a reduced operational range for active and passive devices. While this behaviour is visible across the whole considered range for the TT, higher permitted acceleration and deceleration values do not translate into increased energy consumption or reduced operational range for the straddle carrier (SC) after exceeding an increase of 20 % compared to the base value. Due to the much higher overall weight of the SC compared to the TT, the power limits applied during the driving cycle generation constrain the effective acceleration, deceleration, and velocity even at lower acceleration values, thereby limiting the impact of more permissive driver settings.

However, while restricting the driver behaviour by the means of limiting acceleration, deceleration and velocity positively affects energy consumption, it also affects the productivity of the vehicle. As illustrated in Fig. C1 for the TT, reducing the acceleration and maximum velocity leads to lower productivity on both terminal types, as vehicles require more time to complete each move. The biggest influence is experienced when the velocity is lowered at the empty terminal. The long, straight road sections on this layout lead to extended periods of driving at low speeds, resulting in an increase in travel time.

The trade-off between reduced productivity and potential energy savings from less aggressive driving must be considered. In this context, effective vehicle management becomes increasingly important. Communication between the driver and other terminal elements enables adjusting the driver's behaviour based on the terminal conditions, e.g., the expected waiting time until the load can be supplied by the quay crane. For example, if the driver is aware that the load will not be ready upon arrival, they can adopt a more energy-efficient driving style without negatively impacting the overall process flow. This form of anticipatory driving can help extend the operational range without compromising productivity.

Aside from the operational optimisation, providing incentives for drivers who adopt energy-efficient driving strategies can contribute to lowering the energy demand of terminal operations. Moreover, these strategies are not only relevant for zero-emission CHE units. When applied to conventional diesel-powered equipment, they can also lead to fuel savings and thus reduce operating costs.

Lifting related metrics. Reducing the lifting velocity results in an increased operational range. However, unlike for the driving velocity, this effect is not primarily caused by the energy demand of the lifting process itself. The actual reason for the increase in operational range under the assumed conditions lies in the increased duration of each lifting cycle. An increase in lifting duration results in a larger proportion of the total operation time being allocated to the lifting phase, thereby reducing the time available for driving over the course of a shift. As driving movements cause higher losses and allow only for a lower share of regenerative energy recovery [11], reducing the lifting velocity effectively increases the time spent in the less energy-intensive phase of operation, thereby extending the operational range.

As with the driving velocity and the driver aggressiveness, lowering the lifting velocity also results in reduced productivity. While it contributes to a higher operational range, the extended cycle time obviously reduces the number of completed moves per hour. However, in contrast to lifting, reducing the driving velocity is a more effective measure for lowering the energy consumption. Therefore, a more suitable strategy is to reduce driving speed while maintaining the lifting velocity. This approach improves the operational range by targeting the more energy-intensive driving phase, while not reducing the maximum achievable overall productivity too much.

The influence of the driving share is also visible when the influence of the assigned quay crane is analysed (Fig. D1). The SC achieves the highest operational range when it is assigned to a centrally located quay crane (STS F). This is due to shorter average driving distances, which reduce the time required to complete each move. Consequently, a greater share of the operation is spent in the lifting phase, while the proportion of time spent driving is reduced. Therefore, assignment of SCs to a specific job and the routing of the vehicles influence the energy consumption and the operational range of the vehicles. This finding is consistent with observations reported in [15].

Comparison with literature. In the absence of open-source experimental data for hydrogen-powered straddle carriers, the proposed model was validated through cross-referencing with a comprehensive literature benchmark. The simulated hydrogen consumption for the terminal tractor (0.7 to 1.7 kg/h) and the straddle carrier (2.4 to 3.6 kg/h) aligns with the lower end of the energy-equivalent ranges reported in previous studies and manufacturer specifications. Furthermore, the terminal tractor sub-model utilises vehicle parameters derived from previously validated models. While proprietary internal vehicle parameters remain confidential for many manufacturers, the close alignment of our results with the spectrum presented in Fig. 1 verifies that the

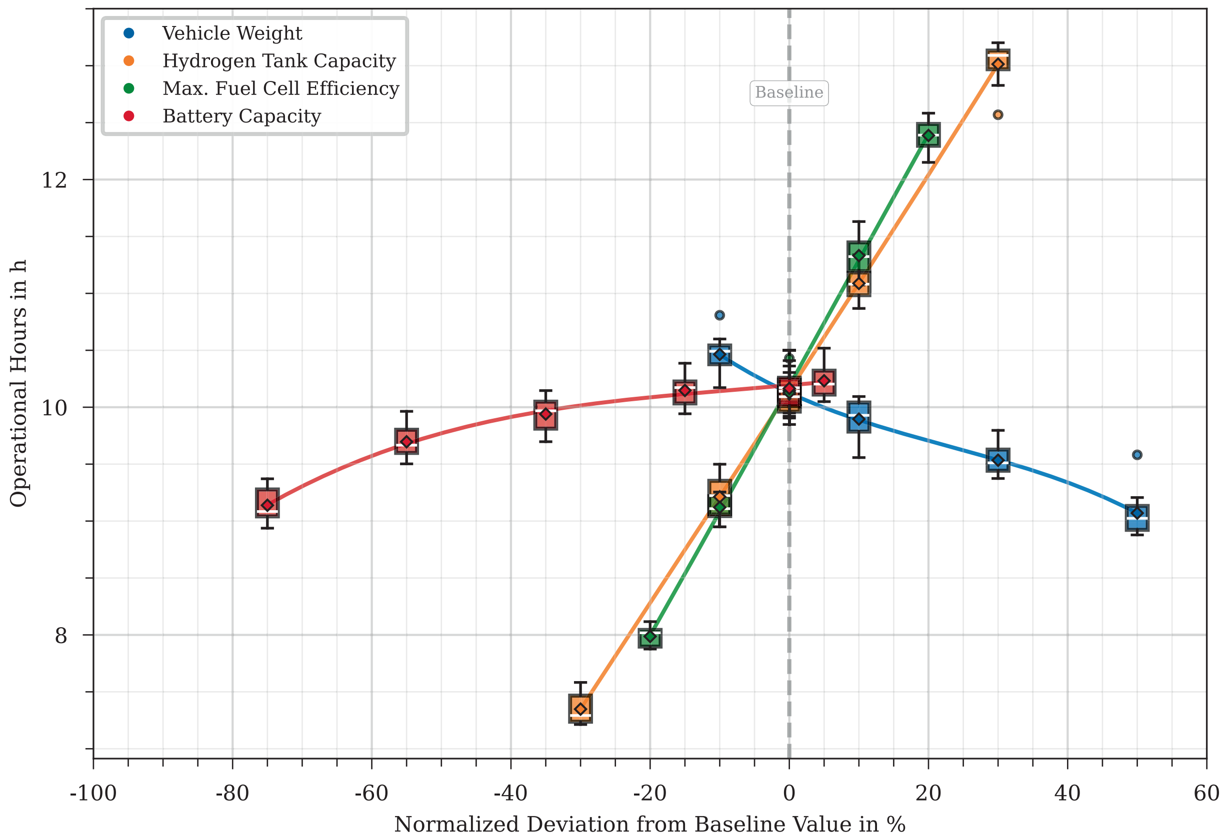

Fig. 8. Influence of vehicle specifications on the operational range of a terminal tractor on a flat field terminal. The box plots represent the results of 10 independent iterations.

physics-based simulation accurately reflects the magnitude of energy demand in real-world port environments.

Finally, the variance in energy demand observed across different use cases highlights a critical industry challenge. Since consumption values and operational runtimes are highly sensitive to specific boundary conditions, such as terminal topology and driver behaviour, communicating single 'average' consumption figures without explicitly defining these operating parameters is of limited value. This underscores the urgent need for standardised assessment frameworks, whether through defined physical testing cycles (similar to VECTO or WLTP) or uniform simulation methodologies where identical boundary conditions are applied to all options. Establishing such standards is essential to enable transparent comparisons between different zero-emission solutions.

4.2. Device specifications

To examine the effects of different vehicle configurations, the analysis is conducted solely for a passive device, represented by a terminal tractor, as similar trends are expected for active equipment.

4.2.1. Results

Fig. 8 and Fig. 9 illustrate the influence of the investigated vehicle specification parameters on the operational range of the terminal tractor for the flat field and the empty terminal, respectively.

An increase in vehicle weight reduces the operational range, while an increased hydrogen tank capacity and an improved fuel cell efficiency result in longer runtimes. The scenario with the lowest considered tank size on the flat field terminal is the only scenario where the defined minimum operational range is not achieved. The impact of battery capacity is more limited and depends on the terminal layout. For the flat field terminal, an increased battery capacity leads to a slightly higher operational range, while on the empty terminal, reducing or increasing the battery size results in an extended operational range.

4.2.2. Discussion

Vehicle weight. An increase in vehicle weight reduces the operational range, consistent with the earlier findings on the payload influence (Section 4.1.2). While the payload is fixed, reducing the vehicle's own weight can help lower the overall energy demand and thus improve the operational range, complementing the constraints imposed by the payload.

Hydrogen tank size. Since the vehicle's hourly energy consumption remains nearly constant within a given use case, apart from the already mentioned randomness in the system, a higher fuel capacity directly translates into longer runtimes. However, tank size is often constrained by the vehicle design and thus the available installation space. In addition, a bigger tank increases the vehicle weight and thus most likely the energy consumption. While a larger tank can support longer shifts without refuelling, the smallest considered tank size does not provide sufficient range to meet the assumed 8 h continuous operation requirement on the flat field terminal. But this smaller tank size is still adequate in other cases with less demanding operational profiles, such as on the empty container terminal when assuming that refuelling can occur during scheduled breaks (Fig. 9).

Fuel cell efficiency. Similar to the tank size, increasing the fuel cell efficiency also results in a linear increase in the operational range, as less

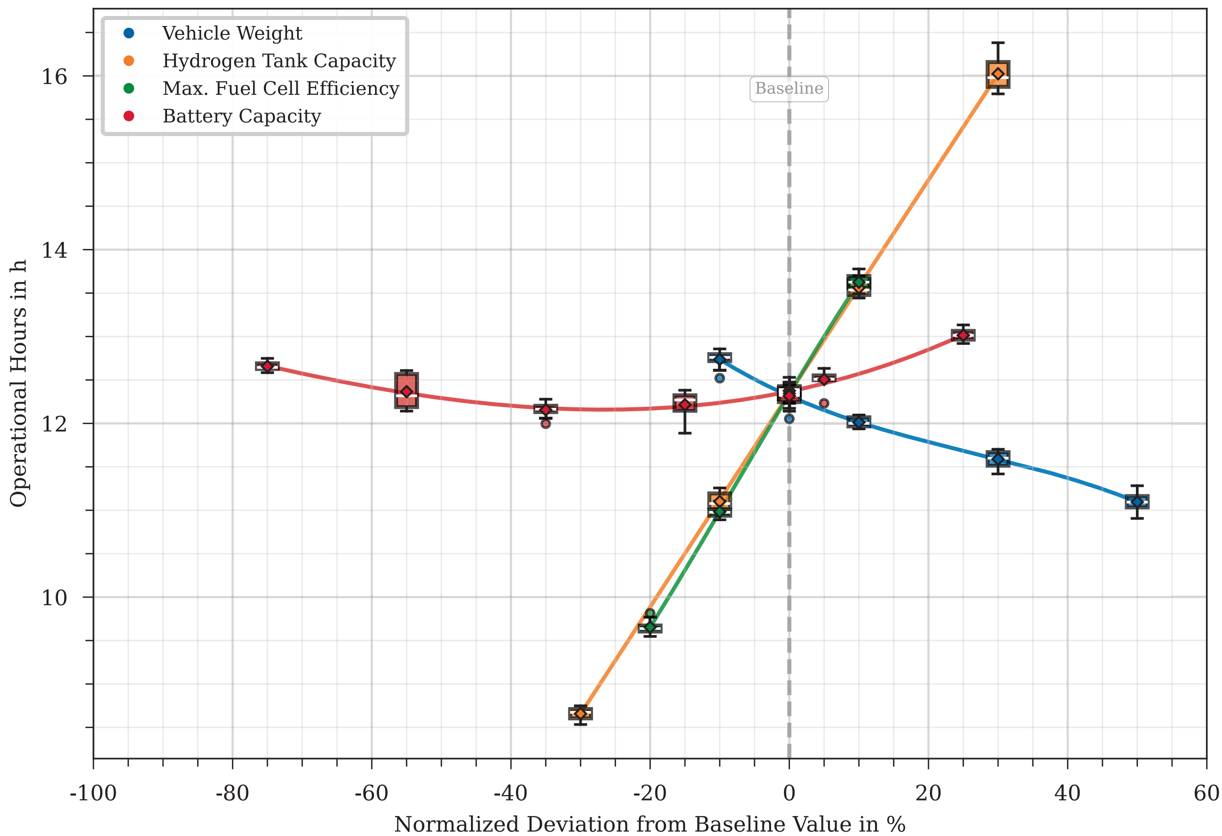

Fig. 9. Influence of vehicle specifications on the operational range of a terminal tractor on an empty container terminal. The box plots represent the results of 10 independent iterations.

hydrogen is required per kWh of electrical energy. These results underline the potential of technological advancements in fuel cell systems to enhance zero-emission operations.

Fuel cell efficiency improvements can be achieved not only by raising the maximum fuel cell efficiency. It is also necessary to implement an energy management strategy suitable for the application of the vehicle in order to operate the fuel cell at high efficiency. In addition to the energy management strategy, the configuration of the device must be tailored to the application, especially regarding the hydrogen tank capacity, fuel cell rated power and battery sizing.

Battery capacity and energy management strategy. The battery primarily serves as a buffer for power peaks and for capturing regenerative braking energy [46]. This system element is not intended to increase the vehicle's driving range, as this would require the availability of electrical charging infrastructure at the terminal.

On the empty terminal, the fuel cell's power output at its optimal operating point exceeds the average power demand. As a result, the upper battery state of charge (SOC) limit permitted by the energy management strategy (EMS) can be reached. A smaller battery stores less energy, thereby reducing the amount of hydrogen required to charge it. This leads to increased runtimes when the battery capacity is reduced compared to the baseline scenario.

On the flat terminal, a reverse effect is observed. Due to the higher mean power request compared to the empty terminal, the fuel cell is unable to supply the mean power request at its optimal operating point under the considered EMS. Increasing the battery capacity enables more energy to be drawn from the battery until the lower SOC limit is reached, thereby extending the range. Increasing the battery capacity beyond the baseline on the empty terminal also leads to an increase in operational range. The EMS enables the fuel cell to operate at its optimal point more frequently, allowing the SOC to be maintained near its desired level. Higher fuel cell efficiencies, combined with the reduced need to recharge the battery, contribute to the improved operational range.

These findings highlight the importance of selecting an optimal vehicle configuration tailored to the specific application. While a larger battery may be beneficial in scenarios with sustained high power demands, such as ship loading at a roll-on/roll-off terminal, it is not universally advantageous. A larger battery increases vehicle costs, adds weight, and reduces the space available for other components, such as a larger hydrogen tank. For the operating conditions analysed on the empty and flat field terminals, a smaller battery is therefore preferable. The operational range increase can be achieved more efficiently by selecting the fuel cell size and designing the EMS to match the specific application requirements.

The modular and universal architecture of this simulation framework provides a robust foundation for identifying such optimal designs. While the current study focus is on assessing the feasibility of configurations currently available on the market, the framework could be integrated into future optimisation loops to develop tailored zero-emission equipment configurations.

5. Conclusion

To enable a broader adoption of zero-emission container handling equipment (CHE) in the future, several key prerequisites have to be fulfilled: technological readiness, operational feasibility, and economic viability. This work addresses the operational feasibility of hydrogen-fuelled container handling equipment. Thus, the primary objective is to identify the key parameters and conditions determining whether zero-emission configurations currently available on the market can serve as viable alternatives to conventional diesel-powered equipment.

To answer this question, a novel method for the estimation of the energy consumption of container handling equipment is presented, enabling the systematic analysis of how different operational conditions and vehicle specifications affect the energy demand and, therefore, the operational range. By describing container terminals as graph networks, the method facilitates the generation of generic driving cycles for CHE units. This allows for the evaluation of multiple use cases without the need to collect test data for each scenario, thereby reducing the effort and cost typically associated with such investigations.

The analysis is conducted for a terminal tractor operating on a flat field and an empty terminal, and a straddle carrier operating on the flat field terminal. The key findings of this analysis can be summarised as follows.

- The investigated fuel cell electric CHE configurations can meet the minimum required operational range.
- Driver behaviour significantly impacts energy consumption. Limiting acceleration, deceleration and velocity of CHE units can substantially increase the operational range and thereby improve the feasibility of alternative powertrains. However, limiting the driver behaviour also reduces the maximum equipment productivity. This trade-off highlights the importance of coordinated terminal operations.
- The specific characteristics of a terminal, such as its layout and the payloads, emerged as critical factors influencing the vehicle energy demand. These site-specific conditions can alter vehicle utilisation patterns and driving distances, and must therefore be considered when evaluating the feasibility of zero-emission CHE deployment. In addition, the wide dispersion of results emphasises that stating energy consumption or runtime values without a precise definition of operating conditions is insufficient.
- The operational range requirement is set so that the vehicles are able to run for at least one 8 h shift. In multi-shift operation, this assumes that the hydrogen tanks can be completely refuelled during designated breaks. This highlights the need for the presence of a sufficient refuelling infrastructure.

Building on these findings, future research should further explore how the identified measures, such as adjusted driver behaviour, can support the operational feasibility of zero-emission vehicles on a larger scale. This includes assessing how charging or refuelling events influence required fleet sizes (i.e., the need for additional vehicles to compensate for those temporarily unavailable) and whether operational requirements can still be met when entire fleets are converted to zero-emission powertrains under the constraints of limited refuelling infrastructure. Looking ahead, assessing the economic feasibility of zero-emission vehicles will also be crucial, as only a combination of the operational and economic feasibility can substantiate the case for large-scale fleet replacement.

Declaration of generative AI and AI-assisted technologies in the writing process

During the preparation of this work, the authors used Anthropic Claude, Google Gemini and OpenAI's ChatGPT in order to improve the readability and language clarity of the manuscript. After using these tools, the authors reviewed and edited the content as needed and take full responsibility for the content of the published article.

CRediT authorship contribution statement

Tobias Prieß: Writing – original draft, Visualization, Software, Methodology, Formal analysis, Data curation. **Luka Bornemann:** Writing – review & editing, Conceptualization. **Martin Kaltschmitt:** Writing – review & editing, Supervision, Funding acquisition, Conceptualization.

Declaration of competing interest

The authors declare that they have no known competing financial interests or personal relationships that could have appeared to influence the work reported in this paper.

Acknowledgements

This research was carried out in cooperation with the Clean Port & Logistics (CPL) cluster. Open Access funding enabled and organised by project DEAL.

Appendix A. Example driving cycles

This appendix presents example driving cycles for both investigated device types, the terminal tractor and the straddle carrier, to visually complement the methodological description in Section 2 and the results discussed in Section 4. The cycles illustrate profiles of vehicle mass, driving speed, traction power, lifting speed and power (for the straddle carrier), as well as the power contributions of the fuel cell and battery over time. Each plot covers 5 moves. For the terminal tractor, example cycles are shown for both reference terminals, i.e., the flat field terminal and the empty container terminal, thereby highlighting how differences in terminal layout and use cases translate into distinct operational patterns and energy demand.

A.1. Terminal Tractor

To illustrate the operational differences between the terminal types discussed in Section 4.1, representative driving cycles for a terminal tractor operating on both the flat field and empty container terminals are presented below. These examples demonstrate the characteristic patterns of vehicle operation under base case conditions, highlighting the key distinctions in power demand, cycle duration, and operational behaviour between the two terminal configurations.

Flat field terminal. Fig. A1 presents driving cycles for five consecutive moves for a 4x2 terminal tractor operating at the flat field terminal, transporting out-of-gauge (OOG) cargo between the OOG, train, and quay sections. The total vehicle mass varies between ca. 12 t (unladen with gooseneck), 20 t (laden with bomb-cart trailer and gooseneck) and 40 t (laden with bomb-cart trailer, gooseneck, and OOG cargo).

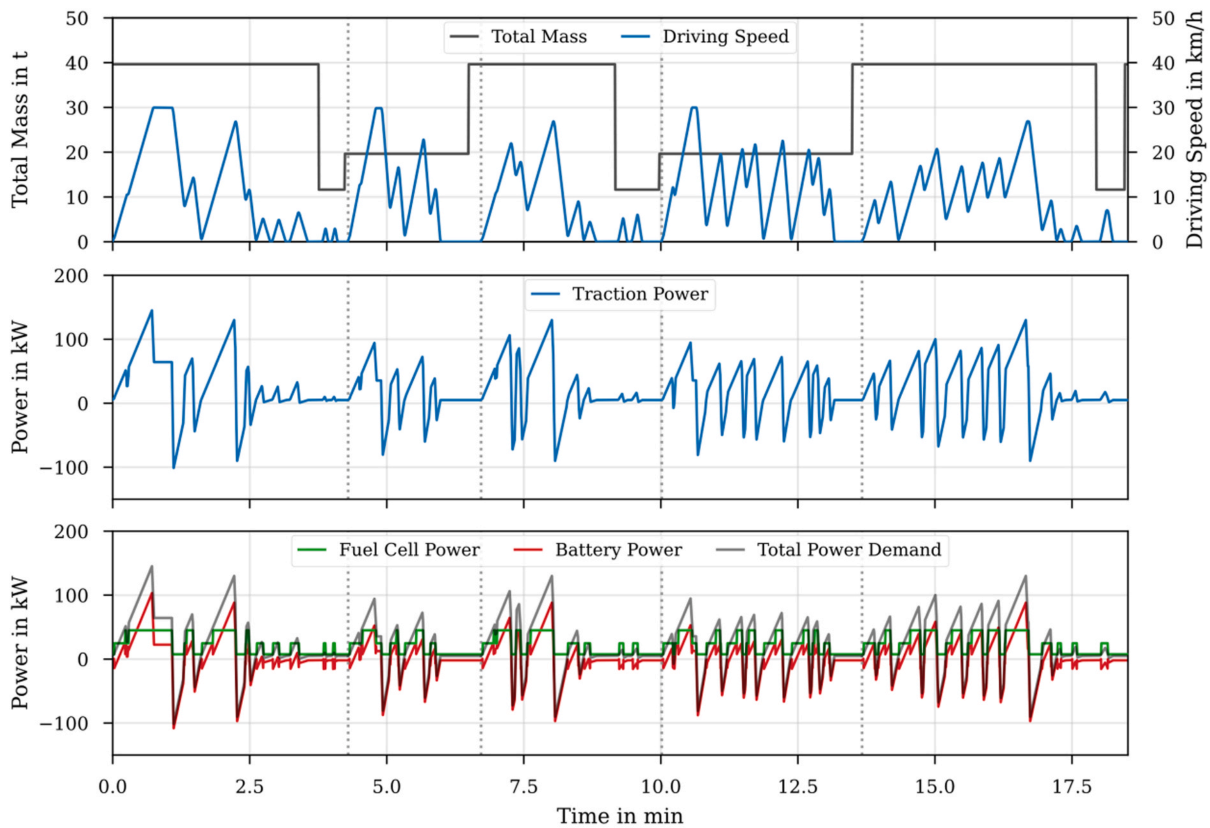

Fig. A1. Driving cycle for 5 consecutive moves of the terminal tractor operating at the flat field terminal (moves separated by dotted lines). Positive values in the middle panel indicate power demand, negative values indicate regeneration. In the lower panel, positive values represent energy supply for the power sources and demand for the total power.

The cycles exhibit frequent velocity variations and relatively short intervals at maximum speed. The flat field terminal's layout, characterised by more frequent cornering, results in pronounced acceleration and deceleration events. The traction power demand profile shows considerable variability, with frequent power peaks and transient load conditions. Regenerative braking during deceleration events is evident from the negative power peaks in the middle panel, which are captured by the battery as shown in the lower panel. Individual moves are generally short in duration, typically ranging from 2 to 4 min.

Empty container terminal. Fig. A2 shows five consecutive driving cycles for the same 4x2 terminal tractor configuration operating at the empty container terminal. The vehicle transfers empty containers between the two yard areas, with the total vehicle mass alternating between ca. 11 t (unladen with chassis) and 15 t (laden with empty container and chassis).

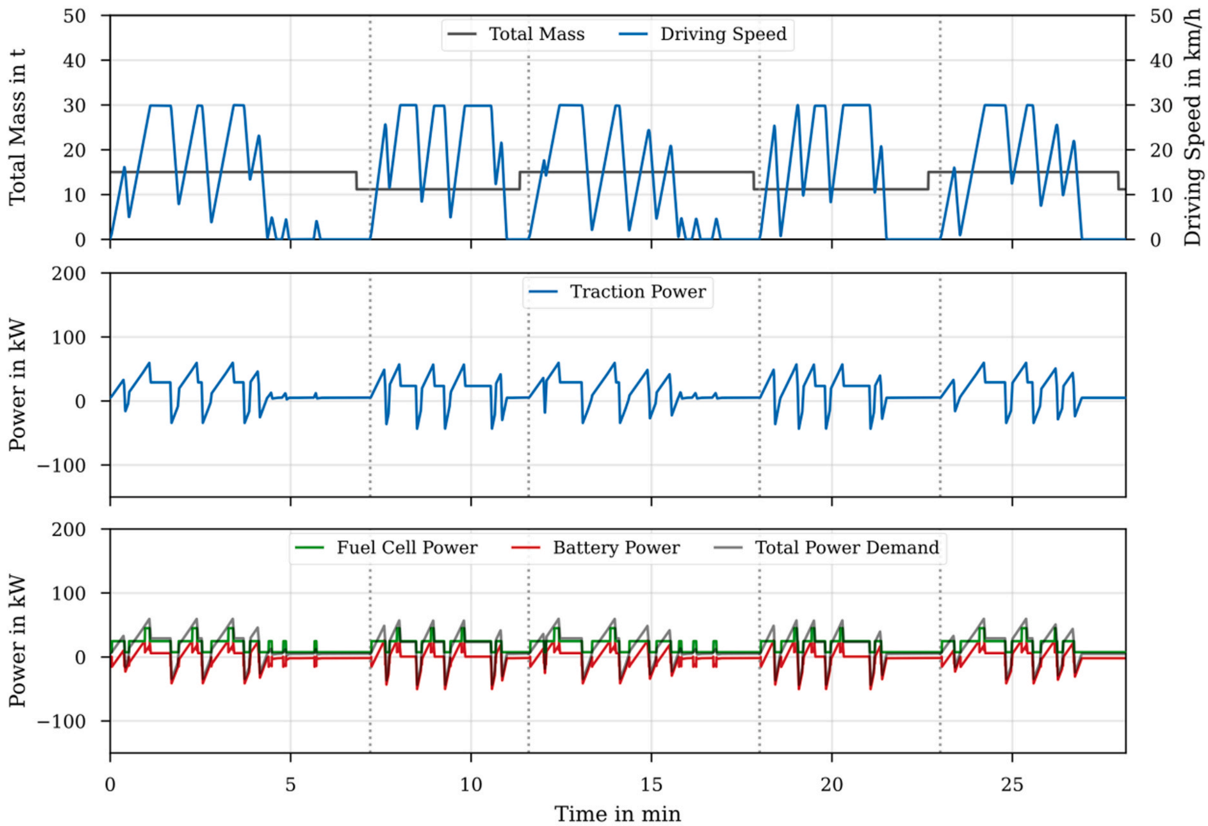

Fig. A2. Driving cycle for 5 consecutive moves of the terminal tractor operating at the empty container terminal (moves separated by dotted lines). Positive values in the middle panel indicate power demand, negative values indicate regeneration. In the lower panel, positive values represent energy supply for the power sources and demand for the total power.

These cycles are characterised by extended periods at maximum velocity (30 km/h), facilitated by the terminal's long, straight road sections. These prolonged high-speed phases result in relatively steady traction power demands, with the fuel cell operating predominantly at consistent output levels. The individual moves vary in duration, ranging from approximately 3 to 7 min due to the considered queuing behaviour.

Main differences between the terminal types. The comparison between the two terminals reveals several key operational differences that influence energy consumption and operational range, as discussed in Section 4.1.2.

- Time at maximum velocity: The empty container terminal allows for significantly longer periods at maximum velocity due to straight road sections, whilst the flat field terminal requires more frequent speed adjustments.
- Move duration: Individual moves at the empty container terminal are generally longer due to the longer driving distances.
- Vehicle weight: The empty container terminal operates with lighter payloads and lower trailer weight, compared to the flat field terminal. This reduced total vehicle mass contributes to lower energy consumption.

A.2. Straddle Carrier

Fig. A3 shows five consecutive operating cycles for a straddle carrier at the flat field terminal. The vehicle performs container transfers between the quay cranes and the straddle carrier yard, including both horizontal transport and vertical lifting operations. The total vehicle mass alternates between ca. 72 t (unladen) and 95 t (laden with a full container).

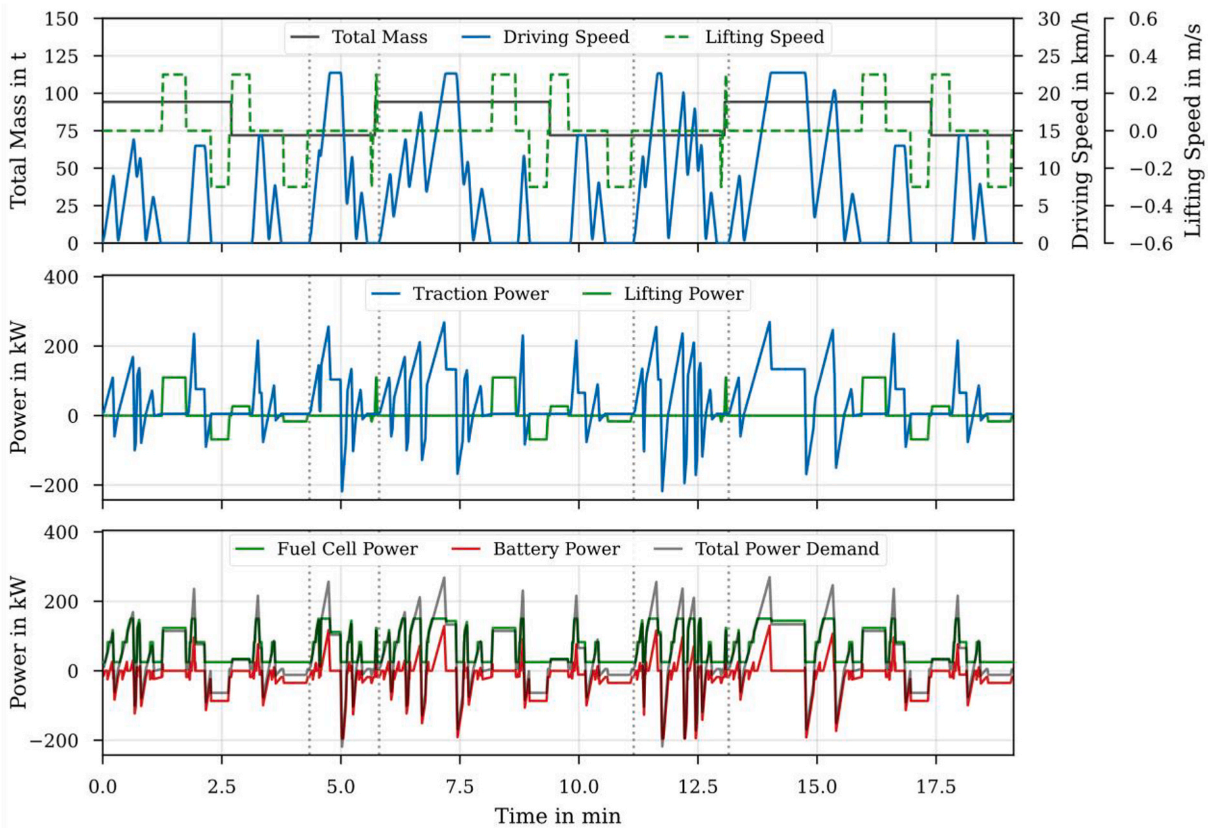

Fig. A3. Driving cycle for 5 consecutive moves of the straddle carrier operating at the flat field terminal (moves separated by dotted lines). Positive values in the middle panel indicate power demand, negative values indicate regeneration. In the lower panel, positive values represent energy supply for the power sources and demand for the total power.

The upper panel displays both the driving speed and lifting speed profiles, with lifting operations clearly visible as variations in the lifting speed. When retrieving or stacking containers in the yard (moves 1, 3, and 5), the straddle carrier lifts the spreader to maximum height to avoid collisions with stacked containers, drives to the pick-up or drop-off location, places or takes the container, exits the yard, and then lowers the spreader to driving height before completing the move. The middle panels show the traction power and lifting power separately, illustrating that lifting operations contribute significantly to the total energy demand. The lower panel demonstrates how the fuel cell and battery share the power supply.

B. Equivalent hydrogen consumption

To access the hydrogen consumption of fuel cell electric vehicles, the battery state of charge (SOC) variation needs to be considered. To account for the energy contribution of the battery, the equivalent hydrogen consumption $m_{H2,eq}$ is considered in this work [47]:

$$m_{H2,eq} = m_{H2} - \frac{\Delta E_b}{\eta_b \cdot \eta_{FC} \cdot LHV_{H2}} \tag{B 1}$$

Here, m_{H2} denotes the actual hydrogen consumption, which is corrected by the battery energy change ΔE_b. A positive sign denotes an increase of the SOC during the operation. Additionally, the maximum fuel cell efficiency η_{FC}, the battery efficiency η_b and the lower heating value of hydrogen, LHV_{H2} are taken into account.

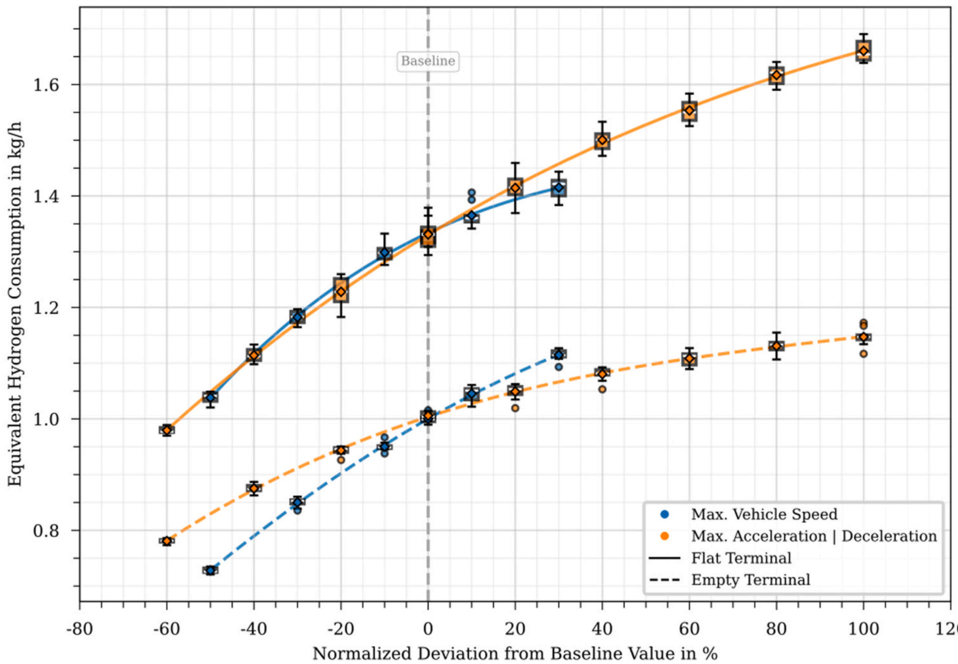

Fig. B1. Equivalent hydrogen consumption for a 4x2 terminal tractor under varying acceleration and vehicle speed boundaries on flat and empty terminals. The box plots represent the results of 10 independent iterations.

Fig. B1 shows the range of the equivalent hydrogen consumption for the 4x2 terminal tractor on the empty and flat terminals for different driver behaviour conditions.

Fig. B2 shows the range of the equivalent hydrogen consumption for the straddle carrier under different driver behaviour conditions.

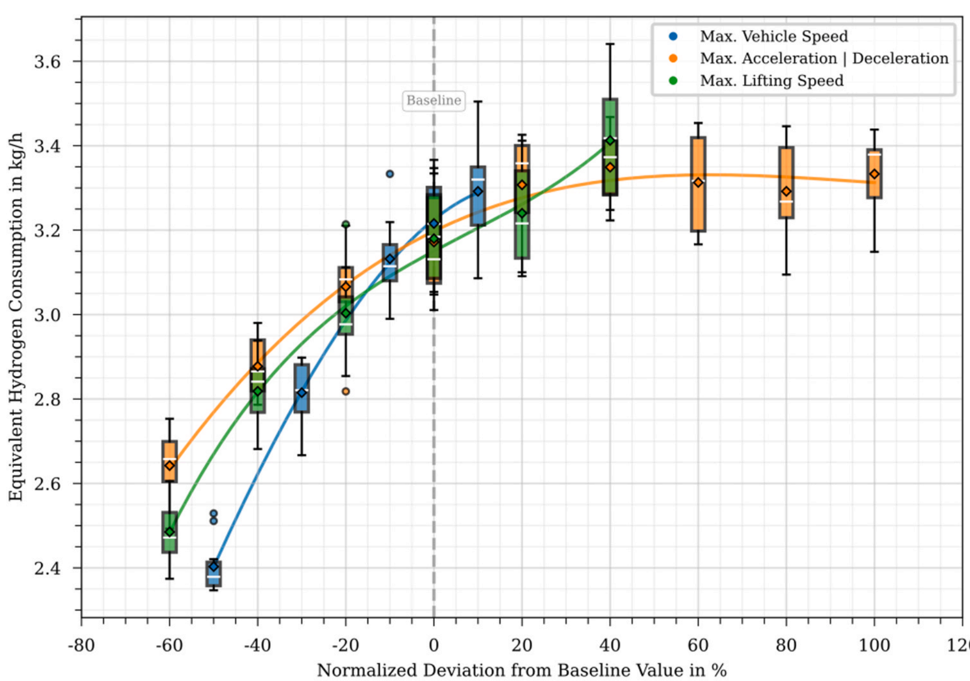

Fig. B2. Equivalent hydrogen consumption for a straddle carrier under varying acceleration, vehicle speed and lifting velocity boundaries. The box plots represent the results of 10 independent iterations.

C. CHE unit productivity

Fig. C1 illustrates the influence of maximum velocity and driver behaviour on the productivity of a 4x2 terminal tractor on both a flat field and an empty container terminal. Productivity is expressed as the number of moves per hour, where one move is defined as a driving cycle from a start to an end node, followed by the operational cycle at the destination.

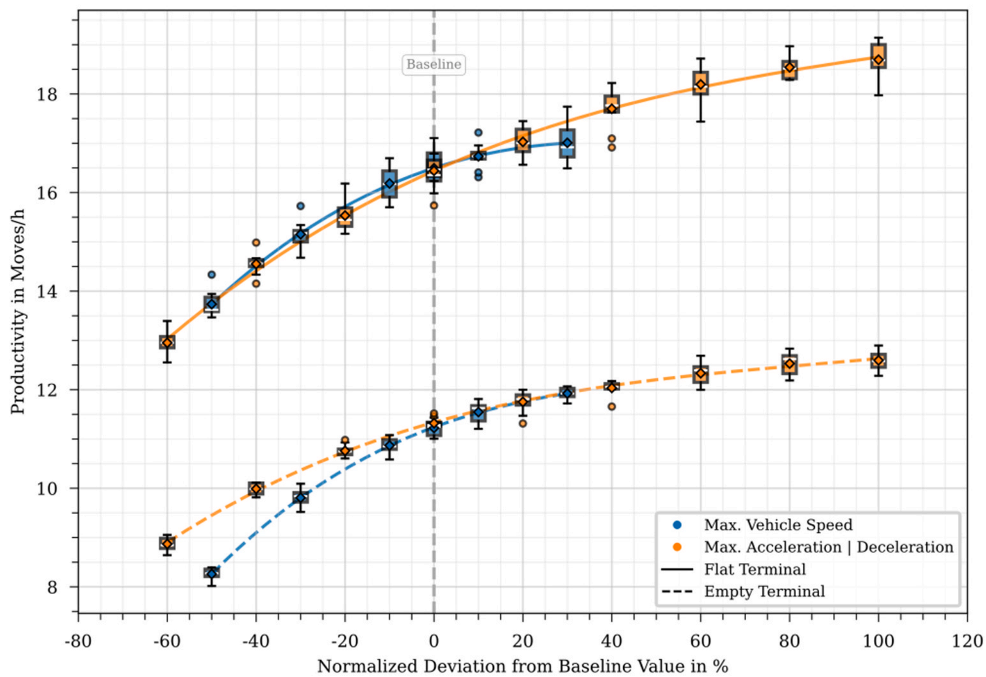

Fig. C1. Influence of the driver behaviour on the number of moves of a terminal tractor on a flat field and an empty container terminal. The box plots represent the results of 10 independent iterations.

D. Influence of the assigned quay crane

An additional factor influencing the energy consumption of the straddle carrier (SC), which does not play a role for the terminal tractor, is the assignment of the vehicle to a specific quay crane (STS). Since the vehicle alternates between the STS and the yard and train sections, the length of each driving step depends on the location of the assigned STS. This effect is illustrated in Fig. D1. Among the analysed configurations, the SC assigned to the centrally located STS F achieves the highest operational range. As expected, limiting the velocity leads to an increased operational range in all cases.

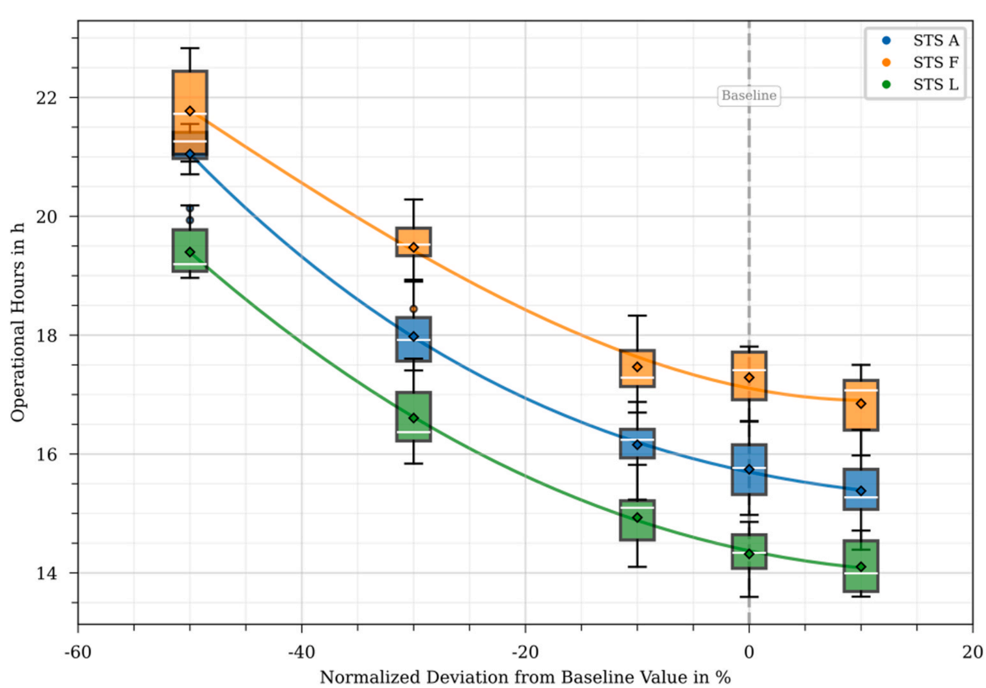

Fig. D1. Influence of the assigned STS and the maximum allowed velocity on the operational range of a straddle carrier. The box plots represent the results of 10 independent iterations.

Data availability

Data will be made available on request.

References

[1] Ramboll. Studie Alternative Antriebe für Hafenumschlaggeräte: Abschlussbericht. 2022.
[2] APM Terminals, DP World. Reaching a tipping point in Battery-Electric Container Handling Equipment. 2023.
[3] Driesch P. Modellgestützte Bewertung des Einsatzes von alternativen Antrieben für Flotten von mobilen Maschinen am Beispiel erdgasbetriebener Terminaltraktoren. Dissertation Universität Duisburg-Essen 2022.
[4] Schmidt-Ewig J, Aldejohann S, Eckstein L, Gerigk M, Martens T, Drope N, et al. Gemeinsamer Abschlussbericht des Konsortiums zum Projekt „ZETT – Zero Emission Terminal Tractor“. RWTH Aachen, BMZ Germany GmbH: Konecranes GmbH; 2021.
[5] Semchukova V, Topolski K, Abdin Z. Hydrogen technology for maritime applications: A review of challenges, opportunities, and lessons from the port authority of New York and New Jersey. Renew Sustain Energy Rev 2025;216: 115641. https://doi.org/10.1016/j.rser.2025.115641.
[6] Densberger NL, Bachkar K. Towards accelerating the adoption of zero emissions cargo handling technologies in California ports: Lessons learned from the case of the ports of Los Angeles and Long Beach. J Clean Prod 2022;347:131255. https://doi.org/10.1016/j.jclepro.2022.131255.
[7] Forrest K, Mac Kinnon M, Tarroja B, Samuelsen S. Estimating the technical feasibility of fuel cell and battery electric vehicles for the medium and heavy duty sectors in California. Appl Energy 2020;276:115439. https://doi.org/10.1016/j.apenergy.2020.115439.
[8] Link S, Plötz P. Technical feasibility of heavy-duty battery-electric trucks for urban and regional delivery in germany - A real-world case Study. World Electr Veh J 2022;13:161. https://doi.org/10.3390/wevj13090161.
[9] Tanvir S, Un-Noor F, Boriboonsomsin K, Gao Z. Feasibility of operating a heavy-duty battery electric truck fleet for drayage applications. Transp Res Rec J Transp Res Board 2021;2675:258–68. https://doi.org/10.1177/0361198120957325.
[10] Pardhi S, Chakraborty S, Tran D-D, El Baghdadi M, Wilkins S, Hegazy O. A review of fuel cell powertrains for long-haul heavy-duty vehicles: technology, hydrogen. Energy and Thermal Management Solutions Energies 2022;15:9557. https://doi.org/10.3390/en15249557.
[11] Kukkaro J. Straddle Carrier electric powertrain optimisation. Tampere University of Technology; 2017. Master thesis.
[12] Di Ilio G, Di Giorgio P, Tribioli L, Bella G, Jannelli E. Preliminary design of a fuel cell/battery hybrid powertrain for a heavy-duty yard truck for port logistics. Energy Convers Manag 2021;243:114423. https://doi.org/10.1016/j.enconman.2021.114423.
[13] Di Ilio G, Di Giorgio P, Tribioli L, Cigolotti V, Bella G, Jannelli E. Assessment of a Hydrogen-Fueled Heavy-Duty Yard Truck for Roll-On and Roll-Off Port Operations 2021. https://doi.org/10.4271/2021-24-0109.
[14] Semchukova V, Polemis K, Abdin Z, Solanki B, Cary S. Hydrogen infrastructure analysis for port applications. National renewable energy. Laboratory 2024.
[15] Hangga P, Shinoda T. Motion-based energy analysis methodology for hybrid straddle carrier towards eco-friendly container handling system. J East Asia Soc Transp Stud 2015;11.
[16] Energy GTI. Zero- and near zero-emission freight facilities project. Zero Emissions for California Ports (ZECAP) 2023.
[17] Pivetta D, Volpato G, Carraro G, Dall'Armi C, Da Lio L, Lazzaretto A, et al. Optimal decarbonization strategies for an industrial port area by using hydrogen as energy carrier. Int J Hydrog Energy 2024;52:1084–103. https://doi.org/10.1016/j.ijhydene.2023.07.008.
[18] Tetra Tech, Gladstein, Neandross & Associates. San Pedro Bay Ports Clean Air Action Plan 2021 Update: Feasibility Assessment for Cargo-Handling Equipment. 2022.
[19] Clean Hydrogen Joint Undertaking. Study on hydrogen in ports and industrial coastal areas - Case studies. Report 3. Publications Office of the European Union; 2023.
[20] Hickson M. Patrick terminals fremantle – battery electric terminal trucks lessons learned report. Patrick Terminals 2024;No. 2.
[21] Kalmar. Electric Reachstacker ERG450-700 Range 2024.
[22] Kalmar. The Kalmar DCG80 -110 Empty Container Handler range 2022.
[23] Kalmar. Reachstacker for Empty Container Handling DRG100-140 Range 2024.
[24] Sany. Reach Stacker SRSC45E5 n.d.
[25] Sany. Full Electric Empty Container Handler SDCE90K7E5 n.d.
[26] Liebherr-MCCtec Rostock GmbH. Reachstacker LRS 545-27 Toplift n.d.
[27] Port of Hamburg. First delivery of an "all-electric full container stacker" in the Port of Hamburg. Port Hambg 2025. https://www.hafen-hamburg.de/en/press/news/first-delivery-of-an-all-electric-full-container-stacker-in-the-port-of-hamburg/ (accessed February 6, 2025).
[28] Johansson P-E, Nurmela M, Bærentzen MK. Hydrogen fuel cell technology in container handling equipment: Industry outlook and technical considerations. Kalmar; 2022.
[29] Xiao Z, Dui-Jia Z, Jun-Min S. A synthesis of methodologies and practices for developing driving cycles. Energy Procedia 2012;16:1868–73. https://doi.org/10.1016/j.egypro.2012.01.286.
[30] Goeke D, Schneider M. Routing a mixed fleet of electric and conventional vehicles. Eur J Oper Res 2015;245:81–99. https://doi.org/10.1016/j.ejor.2015.01.049.
[31] Hulagu S, Celikoglu HB. An electric vehicle routing problem with intermediate nodes for shuttle fleets. IEEE Trans Intell Transp Syst 2022;23:1223–35. https://doi.org/10.1109/TITS.2020.3023673.
[32] De Cauwer C, Verbeke W, Van Mierlo J, Coosemans T. A model for range estimation and energy-efficient routing of electric vehicles in real-world conditions. IEEE Trans Intell Transp Syst 2020;21:2787–800. https://doi.org/10.1109/TITS.2019.2918019.
[33] Hulagu S, Celikoglu HB. Electric vehicle location routing problem with vehicle motion dynamics-based energy consumption and recovery. IEEE Trans Intell Transp Syst 2022;23:10275–86. https://doi.org/10.1109/TITS.2021.3089675.
[34] Pelletier S, Jabali O, Laporte G. The electric vehicle routing problem with energy consumption uncertainty. Transp Res Part B Methodol 2019;126:225–55. https://doi.org/10.1016/j.trb.2019.06.006.
[35] Dijkstra EW. A note on two problems in connexion with graphs. Numer Math 1959; 1:269–71.
[36] Shao S, Guan W, Bi J. Electric vehicle-routing problem with charging demands and energy consumption. IET Intel Transport Syst 2018;12:202–12. https://doi.org/10.1049/iet-its.2017.0008.
[37] Mohr A, Kastner M, Jahn C. Groundbreaking Challenges of Deploying Battery-Electric Terminal Trucks in Container Terminals. In: Clausen U, Dellbrügge M, editors. Adv. Resilient Sustain. Transp. Proc. 6th Interdiscip. Conf. Prod. Logist. Traffic 2023. 1st ed. 2023, Cham: Springer International Publishing; Imprint Springer; 2023, p. 183–98. https://doi.org/10.1007/978-3-031-28236-2_12.
[38] Ferrara A, Jakubek S, Hametner C. Energy management of heavy-duty fuel cell vehicles in real-world driving scenarios: Robust design of strategies to maximize the hydrogen economy and system lifetime. Energy Convers Manag 2021;232: 113795. https://doi.org/10.1016/j.enconman.2020.113795.
[39] Cheng L, Zhao D, Li T, Wang Y. Modeling and simulation analysis of electric forklift energy prediction management. Energy Rep 2022;8:353–65. https://doi.org/10.1016/j.egyr.2022.03.071.
[40] Bassam AM, Phillips AB, Turnock SR, Wilson PA. An improved energy management strategy for a hybrid fuel cell/battery passenger vessel. Int J Hydrog Energy 2016; 41:22453–64. https://doi.org/10.1016/j.ijhydene.2016.08.049.
[41] Hagberg AA, Schult DA, Swart PJ. Exploring Network Structure, Dynamics, and Function using NetworkX. Proc. Python Sci. Conf., Pasadena, California: SciPy; 2008, p. 11–5. https://doi.org/10.25080/tcwv9851.
[42] McKain DL, Clark N, Atkinson RJ, Luzader ZJ, Rutledge B. Quantification of Yard Hostler activity and the development of a representative yard hostler cycle. SAE Tech Pap 2009; 2009–01–2652.. https://doi.org/10.4271/2009-01-2652.
[43] NuveraFuel Cells. Nuvera E-Serie Fuel Cell Engines 2024.
[44] Brinkmann B. Seehäfen - Planung und Entwurf. Berlin: Springer; 2005.
[45] Driesch P, Weißkopf T, Schramm D. Entwicklung repräsentativer Prüfzyklen für mobile Maschinen auf Grundlage realer Felddaten. Sechste IFToMM –CH. Lienz: Campus Tech; 2020.
[46] Khalatbarisoltani A, Zhou H, Tang X, Kandidayeni M, Boulon L, Hu X. Energy management strategies for fuel cell vehicles: A comprehensive review of the latest progress in modeling, strategies, and future prospects. IEEE Trans Intell Transp Syst 2024;25:14–32. https://doi.org/10.1109/TITS.2023.3309052.
[47] Piras M, De Bellis V, Malfi E, Novella R, Lopez-Juarez M. Hydrogen consumption and durability assessment of fuel cell vehicles in realistic driving. Appl Energy 2024;358:122559. https://doi.org/10.1016/j.apenergy.2023.122559.